ACI 445.1R-12

Report on Torsion in Structural Concrete

Reported by Joint ACI-ASCE Committee 445



American Concrete Institute®

Documents
Document Sharing Hub

Full document details: ACI 445.1R-12

First Printing
April 2013

American Concrete Institute®
Advancing concrete knowledge

Report on Torsion in Structural Concrete

Copyright by the American Concrete Institute, Farmington Hills, MI. All rights reserved. This material may not be reproduced or copied, in whole or part, in any printed, mechanical, electronic, film, or other distribution and storage media, without the written consent of ACI.

The technical committees responsible for ACI committee reports and standards strive to avoid ambiguities, omissions, and errors in these documents. In spite of these efforts, the users of ACI documents occasionally find information or requirements that may be subject to more than one interpretation or may be incomplete or incorrect. Users who have suggestions for the improvement of ACI documents are requested to contact ACI via the errata website at www.concrete.org/committees/errata.asp. Proper use of this document includes periodically checking for errata for the most up-to-date revisions.

ACI committee documents are intended for the use of individuals who are competent to evaluate the significance and limitations of its content and recommendations and who will accept responsibility for the application of the material it contains. Individuals who use this publication in any way assume all risk and accept total responsibility for the application and use of this information.

All information in this publication is provided “as is” without warranty of any kind, either express or implied, including but not limited to, the implied warranties of merchantability, fitness for a particular purpose or non-infringement.

ACI and its members disclaim liability for damages of any kind, including any special, indirect, incidental, or consequential damages, including without limitation, lost revenues or lost profits, which may result from the use of this publication.

It is the responsibility of the user of this document to establish health and safety practices appropriate to the specific circumstances involved with its use. ACI does not make any representations with regard to health and safety issues and the use of this document. The user must determine the applicability of all regulatory limitations before applying the document and must comply with all applicable laws and regulations, including but not limited to, United States Occupational Safety and Health Administration (OSHA) health and safety standards.

Participation by governmental representatives in the work of the American Concrete Institute and in the development of Institute standards does not constitute governmental endorsement of ACI or the standards that it develops.

Order information: ACI documents are available in print, by download, on CD-ROM, through electronic subscription, or reprint and may be obtained by contacting ACI.

Most ACI standards and committee reports are gathered together in the annually revised ACI Manual of Concrete Practice (MCP).

American Concrete Institute
38800 Country Club Drive
Farmington Hills, MI 48331
U.S.A.
Phone: 248-848-3700
Fax: 248-848-3701

www.concrete.org

ISBN-13: 978-0-87031-810-8
ISBN: 0-87031-810-1

Documents
Document Sharing Hub

Full document details: ACI 445.1R-12

ACI 445.1R-12

Report on Torsion in Structural Concrete

Reported by Joint ACI-ASCE Committee 445

Daniel A. Kuchma, Chair

Robert W. Barnes Jr., Secretary

Perry Adebar
Neal S. Anderson
Robert B. Anderson
Mark A. Ascheim
Oguzhan Bayrak
Zdenek P. Bažant
Abdeldjelil Belarbi*†
Evan C. Bentz
John F. Bonacci
Hakim Bouadi
Michael D. Brown
Michael P. Collins
David Darwin
Walter H. Dilger*
Marc O. Eberhard
Catherine E. French
Robert J. Frosch
Gary G. Greene*
Neil M. Hawkins
Thomas T. C. Hsu*
Gary J. Klein
Zhongguo John Ma
Adolfo B. Matamoros
Denis Mitchell
Yi-Lung Mo*
Lawrence C. Novak
Carlos E. Ospina
Stavroula J. Pantazopoulou
Maria A. Polak
Julio A. Ramirez
Karl-Heinz Reineck
David H. Sanders*
Raj Valluvan
James K. Wight

*Subcommittee members who produced this report.
†Subcommittee Chair.

The committee would like to thank the following individuals for their contribution to this report: Mohammad Ali, Neal S. Anderson, Shri Bhide, Michael D. Collins, Maria Cristina Vidigal de Lima, Leonard Elfgren, Christos Karayannis, Liang-Jenq Leu, Mohammad Mansour, Basile Rabbat, Khaldoun Rahal, and Paul Zia.

A clear understanding of the effects of torsion on concrete members is essential to the safe, economical design of reinforced and prestressed concrete members. This report begins with a brief and systematic summary of the 180-year history of torsion of structural concrete members, new and updated theories and their applications, and a historical overview outlining the development of research on torsion of structural concrete members. Historical theories and truss models include classical theories of Navier, Saint-Venant, and Bredt; the three-dimensional (3-D) space truss of Rausch; the equilibrium (plasticity) truss model of Nielson as well as Lampert and Thürlimann; the compression field theory (CFT) by Collins and Mitchell; and the softened truss model (STM) by Hsu and Mo.

This report emphasizes that it is essential to the analysis of torsion in reinforced concrete that members should: 1) satisfy the equilibrium condition (Mohr's stress circle); 2) obey the compatibility condition (Mohr's strain circle); and 3) establish the constitutive relationships of materials such as the "softened" stress-strain relationship of concrete and "smeared" stress-strain relationship of steel bars.

The behavior of members subjected to torsion combined with bending moment, axial load, and shear is discussed. This report deals with design issues, including compatibility torsion, spandrel beams, torsional limit design, open sections, and size effects. The final two chapters are devoted to the detailing requirements of transverse and longitudinal reinforcement in torsional members with detailed, step-by-step design examples for two beams under torsion using ACI (ACI 318-11), European (EC2-04), and Canadian Standards Association (CSA-A23.3-04) standards. Two design examples are given to illustrate the steps involved in torsion design. Design Example 1 is a rectangular reinforced concrete beam under pure torsion, and Design Example 2 is a prestressed concrete girder under combined torsion, shear, and flexure.

Keywords: combined action (loading); compatibility torsion; compression field theory; equilibrium torsion; interaction diagrams; prestressed concrete; reinforced concrete; shear flow zone; skew bending; softened truss model; spandrel beams; struts; torsion detailing; torsion redistribution; warping.

ACI Committee Reports, Guides, and Commentaries are intended for guidance in planning, designing, executing, and inspecting construction. This document is intended for the use of individuals who are competent to evaluate the significance and limitations of its content and recommendations and who will accept responsibility for the application of the material it contains. The American Concrete Institute disclaims any and all responsibility for the stated principles. The Institute shall not be liable for any loss or damage arising therefrom.

Reference to this document shall not be made in contract documents. If items found in this document are desired by the Architect/Engineer to be a part of the contract documents, they shall be restated in mandatory language for incorporation by the Architect/Engineer.

CONTENTS

CHAPTER 1—INTRODUCTION AND SCOPE, p. 2
1.1—Introduction, p. 2
1.2—Scope, p. 3

CHAPTER 2—NOTATION AND DEFINITIONS, p. 3
2.1—Notation, p. 3
2.2—Definitions, p. 5

ACI 445.1R-12 was adopted and published April 2013.

Copyright © 2013, American Concrete Institute.

All rights reserved including rights of reproduction and use in any form or by any means, including the making of copies by any photo process, or by electronic or mechanical device, printed, written, or oral, or recording for sound or visual reproduction or for use in any knowledge or retrieval system or device, unless permission in writing is obtained from the copyright proprietors.

Documents
Document Sharing Hub

Full document details: ACI 445.1R-12

CHAPTER 3—HISTORICAL OVERVIEW OF TORSION THEORIES AND THEORETICAL MODELS, p. 5
3.1—Navier's theory, p. 5
3.2—Thin-tube theory, p. 5
3.3—Historical development of theories for reinforced concrete members subjected to torsion, p. 6
3.4—Concluding remarks, p. 13

CHAPTER 4—BEHAVIOR OF MEMBERS SUBJECTED TO PURE TORSION, p. 13
4.1—General, p. 13
4.2—Plain concrete, p. 13
4.3—Reinforced concrete, p. 15
4.4—Prestressed concrete, p. 17
4.5—High-strength concrete, p. 18
4.6—Concluding remarks, p. 19

CHAPTER 5—ANALYTICAL MODELS FOR PURE TORSION, p. 20
5.1—General, p. 20
5.2—Equilibrium conditions, p. 20
5.3—Compatibility conditions, p. 20
5.4—Stress strain relationships, p. 22
5.5—Compression field theory, p. 23
5.6—Softened truss model, p. 25
5.7—Graphical methods, p. 26

CHAPTER 6—MEMBERS SUBJECTED TO TORSION COMBINED WITH OTHER ACTIONS, p. 28
6.1—General, p. 28
6.2—Torsion and flexure, p. 29
6.3—Torsion and shear, p. 33
6.4—Torsion and axial load, p. 36
6.5—Torsion, shear, and flexure, p. 37

CHAPTER 7—ADDITIONAL DESIGN ISSUES RELATED TO TORSION, p. 39
7.1—General, p. 39
7.2—Compatibility torsion and torsional moment redistribution, p. 39
7.3—Precast spandrel beams, p. 47
7.4—Torsion limit design, p. 48
7.5—Treatment of open sections, p. 51
7.6—Size effect on the strength of concrete beams in torsion, p. 53

CHAPTER 8—DETAILING FOR TORSIONAL MEMBERS, p. 53
8.1—General, p. 53
8.2—Transverse reinforcement, p. 55
8.3—Longitudinal reinforcement, p. 57
8.4—Detailing at supports, p. 58

CHAPTER 9—DESIGN EXAMPLES, p. 59
9.1—Torsion design philosophy, p. 59
9.2—Torsion design procedures, p. 59
9.3—Introduction to design examples, p. 67
9.4—Design Example 1: solid rectangular reinforced concrete beam under pure torsion, p. 67
9.5—Design Example 2: Prestressed concrete box girder under combined torsion, shear, and flexure, p. 74

CHAPTER 10—REFERENCES, p. 86

CHAPTER 1—INTRODUCTION AND SCOPE

1.1—Introduction

Accounting for the effects of torsion is essential to the safe design of structural concrete members, requiring a full knowledge of the effects of torsion and a sound understanding of the analytical models that can easily be used for design. For over three decades, considerable research has been conducted on the behavior of reinforced concrete members under pure torsion and torsion combined with other loadings. Likewise, analytical models have been developed based on the truss model concept. Several of these models were developed to predict the full load history of a member, whereas others are simplified and used only to calculate torsional strength. Many models developed since the 1980s account for softening of diagonally cracked concrete.

This report reviews and summarizes the evolution of torsion design provisions in ACI 318, followed with a summary of the present state of knowledge on torsion for design and analysis of structural concrete beam-type members. Despite a vast amount of research in torsion, provisions of torsion design did not appear in ACI 318 until 1971 (ACI 318-71), although ACI 318-63 included a simple clause regarding detailing for torsion. Code provisions in 1971 were based on Portland Cement Association (PCA) tests (Hsu 1968b).

These provisions were applicable only to rectangular nonprestressed concrete members. In 1995, ACI 318-95 adopted an approach based on a thin-tube, space truss model previously used in the Canadian Standards Association (CSA-A23.3-77) code and the Comité Euro-International du Béton (CEB)-FIP code (1978). This model permitted treatment of sections with arbitrary shape and prestressed concrete (Ghoneim and MacGregor 1993; MacGregor and Ghoneim 1995). The ACI 318-02 code extended the application of the (ACI 318) 1995 torsion provisions to include prestressed hollow sections. ACI 318 allows the use of alternative design methods for torsional members with a cross section aspect ratio of 3 or greater, like the procedures of pre-1995 editions of ACI 318 or the Prestressed Concrete Institute (PCI) method (Zia and Hsu 1978).

This report reviews and summarizes the present state of knowledge on torsion and reviews their use as a framework for design and analysis of structural concrete beam-type members. Chapter 3 presents a historical background outlining the development of research on torsion of structural concrete members. The general behavior of reinforced and prestressed concrete members under pure torsion is discussed in Chapter 4. In Chapter 5, the compression field theory (CFT) and softened truss model (STM) are presented in detail. Chapter 5 also includes a description of two graphical methods (Rahal 2000a,b; Leu and Lee 2000). The behavior of members subjected to torsion combined with shear, flexure,

Documents Document Sharing Hub

American Concrete Institute Copyrighted Material—www.concrete.org

Full document details: ACI 445.1R-12

and axial load is discussed in Chapter 6. Chapter 7 introduces additional design issues related to torsion, such as precast spandrel beams, torsion limit design, size effect, open sections, and torsional moment distribution. Detailing of torsional members is described in Chapter 8. Chapter 9 covers detailed design examples of several beams subjected to torsion using ACI 318, EC2-04, and CSA-A23.3-04 design equations, and additional graphical design methods reported by researchers.

1.2—Scope

Theories presented in this report were developed and verified for building members of typical size. For application to large-scale members, size effects should be considered. They could present a serious safety issue when using the shear strength equations provided in the design standard, which cannot take into account the shear strength reduction in large-scale members caused by loss of aggregate interlock behavior. Experimental information on large-scale torsional members is lacking.

CHAPTER 2—NOTATION AND DEFINITIONS

The material presented is a summary of research carried out worldwide and spanning more than four decades, making unification of the symbols and notations used by the various researchers and design codes a challenge. In some cases, mostly for graphs and figures, the notation is kept as originally published.

2.1—Notation

a = moment arm for bending, mm (in.)
a_c = geometric property index
a_o = depth of equivalent rectangular stress block in concrete strut of torsional member, mm (in.)
A = area of yield surface, mm^2 (in.^{2})
A_{cp} = area enclosed by outside perimeter of concrete cross section, mm^2 (in.^{2})
A_ℓ = total area of longitudinal reinforcement to resist torsion, mm^2 (in.^{2})
A_o = gross area enclosed by shear flow path, mm^2 (in.^{2}) (noted as A_{tb} in Eq. (7.2.6))
A_{oh} = area enclosed by centerline of outermost closed transverse torsional reinforcement, mm^2 (in.^{2})
A_{ps} = area of prestressing reinforcement in flexural tension zone, mm^2 (in.^{2})
A_s = area of nonprestressed longitudinal tension reinforcement, mm^2 (in.^{2})
A_s' = area of longitudinal compression reinforcement, mm^2 (in.^{2})
A_t = area of one leg of a closed stirrup resisting torsion within spacing s, mm^2 (in.^{2}) (noted as A_{tb} in Eq. (7.2.6))
b = width of compression face of member, mm (in.)
b_c = width of stirrups, mm (in.)
B = integral of T_w
C = cross-sectional constant to define torsional properties of a beam
d_v = distance between top and bottom longitudinal reinforcement, mm (in.)
D = cross-sectional depth used in fracture mechanics calculations, mm (in.)
D_0 = size effect constant for computing σ_N for plain concrete section
D_1 = normalized constant to represent characteristic structural dimensions used in fracture mechanics calculations
D_b = size effect constant for computing σ_N for reinforced concrete section
D_c = total energy dissipated on discontinuous concrete yield surface
D_s = total energy dissipated by reinforcement
e = moment arm for torsion, mm (in.)
E_c = modulus of elasticity of concrete, MPa (psi)
E_{ps} = modulus of elasticity of prestressed reinforcement in flexural tension zone, MPa (psi)
E_{ps}' = tangential modulus of Ramberg-Osgood curve at zero load MPa (psi)
E_s = modulus of elasticity of reinforcement and structural steel, MPa (psi)
EJ_w = rigidity of beam under warping torque, N·m^2 (lb-in.^{2})
f_c' = characteristic concrete cylinder compressive strength, MPa (psi)
f_c^* = concrete effective (plastic) compressive stress, MPa (psi)
f_{ck} = characteristic compressive strength of concrete, MPa (psi); $f_{ck} = f_{cm} - 8$ MPa ($f_{ck} = f_{cm} - 1200$ psi)
f_{cm} = mean compressive strength of concrete, MPa (psi)
f_d = diagonal concrete stress, MPa (psi)
f_{ds} = diagonal concrete stress corresponding to strain ε_{ds}, MPa (psi)
f_ℓ = reinforcement stress in ℓ direction, MPa (psi)
$f_{\ell p}$ = prestressing reinforcement stress in the ℓ direction, MPa (psi)
$f_{\ell y}$ = specified yield strength of longitudinal reinforcement, MPa (psi)
f_p = stress in prestressing reinforcement; f_p becomes $f_{\ell p}$ or f_{tp} when applied to longitudinal and transverse reinforcement, respectively, MPa (psi)
$f_{p0.1}$ = characteristic yield strength of prestressing reinforcing strands, MPa (psi); $f_{p0.1} = 0.9f_u$
f_{pc} = compressive stress in concrete due to prestress, MPa (psi)
f_{pk} = characteristic tensile strength of prestressing reinforcing strands, MPa (psi); $f_{pk} = f_{pu}$
f_{po} = effective prestress after losses in prestressing reinforcement, MPa (psi)
f_{pu} = specified tensile strength of prestressing reinforcement, MPa (psi)
$f_{p,ud}$ = design ultimate strength of prestressing reinforcing strands, MPa (psi); $f_{p,ud} = f_{pk}/\gamma_s$ ($\gamma_s = 1.15$)
f_r = modulus of rupture of concrete, MPa (psi)
f_t = reinforcement stress in t direction, MPa (psi)
f_t' = uniaxial tensile strength of concrete, MPa (psi)
f_t^* = concrete effective (plastic) tensile stress, MPa (psi)
f_{tp} = prestressing reinforcement stress in t direction, MPa (psi)

Documents
Document Sharing Hub

American Concrete Institute Copyrighted Material—www.concrete.org

Full document details: ACI 445.1R-12

f_{ty} = specified yield strength of transverse reinforcement, MPa (psi)
f_y = specified yield strength of reinforcement, MPa (psi)
f_{yd} = design yield strength reinforcing steel, MPa (psi); $f_{yd} = f_y/\gamma_s$ ($\gamma_s = 1.15$)
$f_{y\ell}$ = yield strength of the torsional longitudinal reinforcement, MPa (psi)
f_{yv} = torsional hoop yield strength reinforcement, MPa (psi)
G = shear modulus, MPa (psi)
h = overall thickness or height of a member, mm (in.)
H_o = horizontal force in radial direction, N (lb) (Chapter 7)
I_p = polar moment of inertia, mm^4 (in.^{4})
k_1 = ratio of average stress to peak stress
K = value from Mohr-Coulomb yield criterion
K_f = flexural stiffness of floor beams, N·m^2 (lb-in.^{2})
K_{ts} = torsional stiffness of spandrel beam, N·m/rad (in.-lb/rad)
ℓ = span length of beam, mm (in.)
ℓ_f = length of flexural beam, mm (in.)
ℓ_q = width of shear flow q along top wall (Fig. 4.2(a) and (b)), mm (in.)
m = ratio of effective (plastic) compressive stress to effective (plastic) tensile stress of concrete
M = applied flexural moment at section, N·m (in.-lb)
M_o = pure flexural strength of section, N·m (in.-lb)
n = integer value
n_R = number of redundants
n_V = coefficient describing an under-reinforced, partially under-reinforced, or completely over-reinforced section
N = applied axial load at section, N (lb)
N_o = pure axial strength of section, N (lb)
p_h = perimeter of centerline of outermost closed transverse torsional reinforcement, mm (in.)
p_o = perimeter of outer concrete cross section, mm (in.) (sometimes noted as p_{cp})
P = applied concentrated load, N (lb)
q = shear flow, N/m (lb/in.)
r = ratio of top-to-bottom yield forces of the longitudinal reinforcement
r = size effect constant for computing σ_N
R = shape parameter used in Ramberg-Osgood
s = center-to-center spacing of longitudinal and transverse reinforcements, mm (in.)
s_l = center-to-center spacing of longitudinal reinforcement, mm (in.)
s_t = center-to-center spacing of transverse reinforcement, mm (in.)
t = wall thickness of hollow section, mm (in.)
t_d = thickness of shear flow zone, mm (in.)
T = applied torsional moment at section, N·m (in.-lb)
T_c = nominal torsional strength provided by concrete, N·m (in.-lb)
T_{cr} = torsional cracking resistance of cross section, N·m (in.-lb)
T_f = applied torsional moment, N·m (in.-lb) (Chapter 9)
T_{max} = maximum torsional moment, N·m (in.-lb) (Chapter 7)
T_n = nominal torsional moment strength, N·m (in.-lb)
T_o = pure torsional strength of section, N·m (in.-lb)
T_s = nominal torsional strength provided by reinforcement, N·m (in.-lb)
T_u = factored torsional moment at section, N·m (in.-lb)
T_w = warping torsional moment, N·m (in.-lb)
T_{xu} = factored balanced torsional strength, N·m (in.-lb)
T_{xub} = balanced torsional strength, N·m (in.-lb)
$\overline{T}_{xub}$ = nondimensional balanced torsional strength, N·m (in.-lb)
v = shearing stress due to shear, MPa (psi)
v^* = plastic flow rate (Chapter 7)
v_u = ultimate shear stress, MPa (psi)
V = applied shear force at section, N (lb)
V_c = nominal shear strength provided by concrete, N (lb)
V_o = pure shear strength of section, N (lb)
V_u = factored shear force at section, N (lb)
w = ultimate distributed load on helical stair, N/m (lb/ft) (Chapter 7)
W = external work, N/m (lb/ft)
x = shorter overall dimension of rectangular part of cross section, mm (in.)
x_1 = distance section centroid and an infinitesimally small area of yield surface, mm (in.)
y = longer overall dimension of rectangular part of cross section, mm (in.)
z = distance along axis of beam, mm (in.)
α, β = Saint-Venant's coefficients for homogeneous torsional section
α^*, β^* = rotational angles in beam subjected to torsion (Chapter 7)
α_1 = stress block factor given as ratio of f_d to f_c' (Chapter 5)
β = factor relating effect of longitudinal strain on shear strength of concrete (American Association of State Highway and Transportation Officials (AASHTO) LRFD (general message)
β_1 = factor relating depth of equivalent rectangular compressive stress block to neutral axis depth; also, block factor given as ratio of a_o to t_d (Fig. 4.5)
γ_1 = angle along helical stair (in plan) at which maximum torsional moment is assumed to occur
γ_2 = angle along helical stair (in plan) at which vertical moment is assumed to be zero
$\gamma_{\ell t}$ = shear strain
ε_d = strain in d direction
ε_{dec} = strain in prestressing reinforcement at decompression of concrete
ε_{ds} = maximum strain at concrete strut surface (Fig. 4.3)
ε_h = strain in hoop direction ε_ℓ
$\varepsilon_{\ell y}$ = yield strain in ℓ direction
ε_o = strain at peak compressive stress f_c' in concrete
ε_p = peak strain in concrete
ε_r = strain in r direction
ε_s = strain in nonprestressed reinforcement; ε_s becomes ε_ℓ or ε_t when applied to longitudinal or transverse reinforcement, respectively
ε_t = strain in t direction
ε_{ty} = yield strain in t direction

Documents
Document Sharing Hub
American Concrete Institute Copyrighted Material—www.concrete.org
Full document details: ACI 445.1R-12

ε_{uk} = characteristic total elongation of reinforcing steel at ultimate load
ε_x = longitudinal strain at midheight of concrete section
ζ = softening coefficient of concrete strut
η_ℓ = normalized reinforcement ratio of longitudinal reinforcement
η_{lb} = balanced normalized reinforcement ratio of longitudinal reinforcement
η_t = normalized reinforcement ratio of transverse steel reinforcement
η_{tb} = balanced normalized reinforcement ratio of transverse steel reinforcement
θ = angle between axis of strut, compression diagonal, or compression field and tension chord of the member; also, the angle between ℓ-t direction/axis and d-r direction/axis, radians
ξ = coefficient equal to 1 for rectangular sections and to $\pi/4$ for circular cross sections; ξ can be taken as unity for all shapes of cross sections with only negligible loss of accuracy for A_o and p_o
ρ_ℓ = reinforcement ratio in ℓ direction
$\rho_{\ell p}$ = prestressing reinforcement ratio in ℓ direction
ρ_t = reinforcement ratio in t direction
ρ_{tp} = prestressing reinforcement ratio in t direction
σ = compressive stress acting in combination with torsional moment, psi (MPa)
σ_0 = nominal torsional strength according to the current code specifications based on plastic limit analysis, MPa (psi)
σ_d = principal stress in d direction for concrete struts, MPa (psi)
σ_ℓ = normal stress in longitudinal direction for reinforced concrete, MPa (psi)
σ_{max} = maximum principal tensile stress, MPa (psi)
σ_N = nominal strength of structure, MPa (psi)
σ_r = principal stress in r direction for the concrete struts, MPa (psi)
σ_t = normal stress in the transverse direction for reinforced concrete, MPa (psi)
σ_∞ = strength of plain beams according to elastic analysis with maximum stress limited by material strength, MPa (psi)
τ = shearing stress due to torsion and shear, MPa (psi)
τ_{max} = maximum shear stress, MPa (psi)
$\tau_{\ell t}$ = applied shear stress in ℓ-t coordinate for reinforced concrete, MPa (psi)
ν = uniform plastic effectiveness factor (Chapter 7)
ν_c = plastic effectiveness factor for compression (Chapter 7)
ν_t = plastic effectiveness factor for tension (Chapter 7)
φ = friction angle
ϕ = strength reduction factor
ϕ_c = strength reduction factor for concrete (0.65 for cast-in-place, 0.70 for precast concrete)
ϕ_p = strength reduction factor for prestressing tendons (0.90)
ϕ_s = strength reduction factor for nonprestressed reinforcing bars (0.85)
Φ = angle of twist in torsional beam, radians/m (radians/in.)
Φ' = second derivative of rotation with respect to beam's axis z
Φ'' = third derivative of rotation with respect to beam's axis z
Ψ = bending curvature of concrete strut
ω_ℓ = reinforcement index in ℓ direction
ω_s = functional indicator of an index of reinforcement
$\omega_{s\ell}$ = reinforcement ratio index
ω_t = reinforcement index in t direction

2.2—Definitions

ACI provides a comprehensive list of definitions through an online resource, "ACI Concrete Terminology," http://terminology.concrete.org.

CHAPTER 3—HISTORICAL OVERVIEW OF TORSION THEORIES AND THEORETICAL MODELS

3.1—Navier's theory

A theory for torsion of elastic homogeneous members was first developed by C. L. Navier (1826) for circular cross sections. His theory, which was based on equilibrium conditions, compatibility conditions, and a linear stress-strain relationship like Hooke's Law, has guided the development of various theories about the behavior of reinforced concrete members subjected to torsion after cracking.

3.2—Thin-tube theory

Navier's torsion theory for members of circular sections was followed by Saint-Venant's (1856) solution for rectangular sections. Saint-Venant's torsional constants considered warping of rectangular cross sections. According to Saint-Venant's circulatory shear flow theory, the most efficient cross section to resist torsion is a thin tube. Bredt (1896) was able to derive simple equations for thin tubes. His thin-tube theory states that the shear stress multiplied by wall thickness has a constant value around the perimeter and that this shear flow is found by dividing the torsion by twice the area enclosed by the shear flow path. Bredt's theory has served as the basis for modern theories of cracked reinforced concrete members subjected to Saint-Venant torsion.

3.2.1 *Two- and three-dimensional plane truss models*—The first theoretical models for shear in cracked reinforced concrete members date back to the turn of the century when Ritter (1899) and Mörsch (1902) formulated the two-dimensional (2-D) plane truss model concept, where reinforced concrete members were modeled as an assembly of two types of linear elements—concrete struts and reinforcement ties. The axis of concrete struts in the model was assumed to be inclined at 45 degrees to longitudinal members, and shear strength was assumed to be controlled by the yielding of transverse reinforcement ties. By extending the 2-D plane truss model, Rausch (1929) developed a three-dimensional (3-D) space truss model for torsion that consisted of longitudinal and hoop reinforcement-resisting tension and concrete struts-resisting compression. He also assumed that

Documents
Document Sharing Hub

American Concrete Institute Copyrighted Material—www.concrete.org

Full document details: ACI 445.1R-12

the shear flow path would follow the centerline of the hoop reinforcement.

3.2.2 *Skew-bending and space truss theories*—In later years, research on torsion followed two theoretical tracks—skew-bending and space truss. Lessig (1959) first proposed a skew-bending theory for reinforced concrete members with two modes of failure, Mode 1 and Mode 2, as explained in 3.3.5. The skew-bending theory used only equilibrium equations and assumed that all reinforcement yielded before failure. Lessig's research was followed by the skew-bending theory of Walsh et al. (1966) and Collins et al. (1968a,b), who proposed a third failure mode, Mode 3, and used all three modes to derive nondimensional torsion-bending moment interaction equations (Walsh et al. 1967), as described in 3.3.5. Based on three modes of failure, a nondimensional interaction surface of torsion, shear, and flexure was derived by Elfgren (1972a,b) and Elfgren et al. (1974a,b). Rausch's space truss theory for torsion was generalized by Lampert and Thürlimann (1969, 1971), who showed how the angle of inclination of the compression diagonals at failure could be determined from equilibrium if both the hoops and longitudinal reinforcement were assumed to yield. Lampert and Collins (1972) showed that predictions of skew-bending and space truss theories were in close agreement.

3.2.3 *Compression field theory (CFT)*—The truss model with linear elements developed by Rausch was replaced in the 1960s by a new type of truss model with membrane elements that were subjected to in-plane normal and shearing stresses. In determining the torsional strength of members where some reinforcement does not yield, consider compatibility conditions. Such conditions were introduced by Baumann (1972) for shear and by Collins (1973) for torsion. Mitchell and Collins (1974) incorporated compatibility conditions in their CFT, which also relied on equilibrium equations and nonlinear material models for concrete and reinforcement. Unlike previous models, the CFT calculates cracked member torsional behavior up to the peak torque. A compatibility condition derived by minimizing the strain energy in the system is used to calculate the angle of inclination in the truss model struts.

3.2.4 *Softened truss model (STM)*—In 1985, Hsu and Mo (1985a,b,c) proposed the STM by softening the concrete stress-strain curve. All of the aforementioned models satisfy Navier's theory. Earlier models overestimated test strengths (Hsu 1968c), whereas the CFT, which uses spalling of concrete cover, and STM, which uses softening of concrete, have been shown to predict test results accurately (McMullen and El-Degwy 1985).

3.3—Historical development of theories for reinforced concrete members subjected to torsion

3.3.1 *General*—Section 3.1 summarizes the historical models developed to describe reinforced concrete members subjected to torsion, covering almost two centuries of research from 1826 to the early twenty-first century (2007). Classical theories include Navier (1826), Saint-Venant (1856), Bredt (1896), and Bach (1911). This review shows that the three principles of mechanics of materials (equilibrium, compatibility conditions, and materials stress-strain relationships) have been the basis for research in torsion of reinforced concrete members. (Equation notation in this section are provided in Chapter 2.)



Fig. 3.3.2—ACI Committee 438—Torsion, Mexico City, October 1976: Tom Hsu, Lennart Elfgren, Phil Ferguson, Art McMullen, Emory Kemp, Gordon Fisher, Paul Zia, and Michael Collins.

3.3.2 *Twentieth century*—In the first 60 years of the twentieth century, progress in reinforced concrete theories was made primarily on flexure. Early flexural theories for reinforced concrete assumed plane sections remained plane and stress-strain relationships of concrete and reinforcement were linear. Equilibrium conditions for longitudinal stresses were used to determine the location of the neutral axis and stresses in concrete and reinforcement caused by the moment. The contribution of concrete tensile stresses was disregarded if concrete cracking was expected. Later flexural theories accounted for the nonlinear stress-strain response of the concrete and steel reinforcement so that the complete moment-curvature relationship for a section could be predicted. In terms of shear and torsion research, a significant achievement was made with the development of truss models (Ritter 1899; Mörsch 1902; Rausch 1929). Research in torsion of reinforced concrete underwent significant advances during the last 40 years of the twentieth century. Two theories were developed—skew-bending and truss models with membrane elements. Skew-bending includes the theories of Lessig (1959), Yudin (1962), Collins et al. (1968a), Hsu (1968a), and Elfgren (1972a,b). Truss models include the theories of Nielsen (1967), Lampert and Thürlimann (1968, 1969), Collins (1973), Mitchell and Collins (1974), Elfgren et al. (1974a,b), Collins and Mitchell (1980), and Hsu and Mo (1985a,b,c). Several researchers involved in the development of theories for torsion were members of ACI Committee 438 for Torsion, which is now the Joint ACI-ASCE Committee 445 for Shear and Torsion (Fig. 3.3.2).

Development of these modern truss models was based on the same three principles of mechanics, which, in terms of torsion and shear, include the softened stress-strain relationship of concrete.

3.3.3 *Classical torsion theory for homogeneous members*—Navier (1826) derived a theory for torsion of homogeneous elastic members with circular cross sections. His theory is based on the three principles of mechanics of materials:

Document Sharing Hub
American Concrete Institute Copyrighted Material—www.concrete.org
Full document details: ACI 445.1R-12

equilibrium, compatibility conditions, and Hooke's Law. Navier's work also includes the linear theory for flexure. His book is recognized as the first on the mechanics of materials The three principles of the mechanics of materials have become well known as Navier's theory. His theory defines the torsional rigidity for circular sections as GI_p. By extending the formulas for the polar moment of inertia of circular sections to square sections, Navier found that the calculated strength for specimens tested by Duleau (1820) overestimated measured values by approximately 20 percent. He acknowledged that "the formulae for square members do not depict as accurately the behavior as those for circular members." This inconsistency was explained three decades later by Saint-Venant (1856), who recognized that Navier's polar moment of inertia could not reflect the warping deformation of rectangular cross sections. To obtain the correct solution, Saint-Venant developed the semi-inverse method to solve all 15 differential and algebraic equations in the theory of elasticity developed by Cauchy (1828). By satisfying equilibrium, compatibility, and Hooke's Law at each differential element of a member, Saint-Venant developed a solution that considered the warping displacements of rectangular cross sections. In Saint-Venant's rigorous derivation, torsional rigidity is defined as GC. The torsional constant C is taken as $\beta x^3 y$, where the coefficient β is a function of the ratio y/x and varies between 0.141 ($y/x = 1$) and 0.333 ($y/x = \infty$). The maximum shear stress τ_{max} occurs on the outside face of the rectangular section at midpoint of each long side and is equal to $T/\alpha x^2 y$, where α is a coefficient that varies between 0.208 ($y/x = 1$) and 0.333 ($y/x = \infty$). The relationship between α and β is $\alpha = \beta/k$, where

$$k = 1 - \frac{8}{\pi^2} \sum_{n=1,3,5,\ldots}^{\infty} \frac{1}{n^2 \cosh \frac{n\pi y}{2x}}$$

According to Saint-Venant's circulatory shear flow pattern, the maximum shear stresses occur at the outer periphery of a cross section, and the most efficient cross section to resist torsion is a thin tube, as shown in Fig. 3.3.3.

Bredt (1896) was able to derive a simple equilibrium equation for thin tubes by assuming the entire tube to be uniformly and fully stressed

$$q = \frac{T}{2A_o} \tag{3.3.3}$$

The area A_o is formed by sweeping the lever arm (symbol a in Fig. 3.3.3) around the axis of twist, a term later called the "lever arm area" (Hsu 1988). The torsional constant C for thin tubes with constant thickness was also simplified to $C = 4A_o^2 t/p_o$. Bach's formula (1911) is a simplification of Saint-Venant's theory for thin-walled open sections, such as T, L, and I sections. Because the coefficient β for each rectangular component of such sections can be approximated as 1/3, the torsional constant for the entire section can be taken as the sum (Σ) of the components ($C = 1/3\Sigma x^3 y$). The theories of

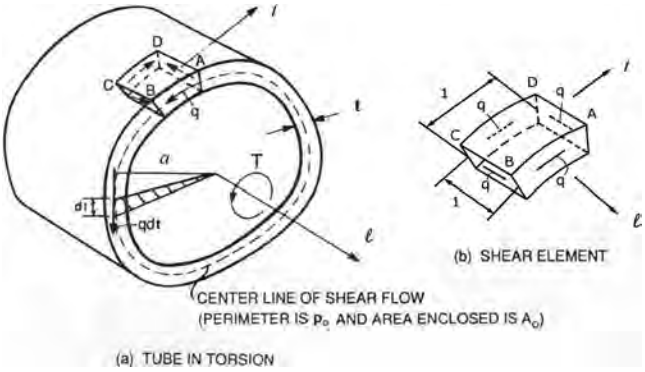


Fig. 3.3.3—Torsion of thin tube and lever arm area A_o (Hsu 1993 after Bredt 1896).

Navier, Saint-Venant, Bredt, and Bach are applicable to reinforced concrete beams before cracking. They also laid the foundation for developing theories to calculate the behavior of cracked reinforced concrete members subjected to torsion.

3.3.4 *Theories for reinforced concrete under flexure, shear, and torsion*—Reinforced concrete was first developed in 1867 when Joseph Monier obtained a patent for reinforcing his concrete flowerpots with wrought iron wires. The concept of using steel reinforcement to overcome the weakness of concrete in tension was quickly adapted to buildings and bridges, making the use of reinforced concrete for construction a widely accepted application in the last quarter of the nineteenth century. Such growth in applications gave rise to the demand for theories to analyze and design reinforced concrete structures.

3.3.4.1 *Flexure theory*—As reported by Delhumeau (1999), the first flexure theory to emerge was the linear flexure theory developed by Hennebique's firm near the end of the nineteenth century. This theory served as the basis for the allowable stress design method addressed in the first ACI code [National Association of Cement Users (NACU) 1910]. Theories for nonlinear flexure occupied the attention of researchers until 1963 when strength design was incorporated in ACI 318 (ACI 318-63). Both linear and nonlinear theories for flexure satisfy the three principles of the mechanics of materials: equilibrium of parallel coplanar forces, Bernoulli's linear strain compatibility, and the constitutive laws of materials. A linear stress-strain curve of reinforcement and concrete is used for the linear flexure theory and a nonlinear stress-strain curve of concrete is used for the nonlinear flexure theory.

3.3.4.2 *Torsion and shear theory*—Following the adoption of flexural strength design in ACI 318-63, the attention of researchers turned to more complex problems of torsion and shear in beams. Computer analysis of structures was becoming available, making it feasible for design engineers to compute the magnitude of torsions in their buildings. In addition, concrete box-girder bridges, which were becoming a competitive bridge type, needed to be designed for torsion. Shear is essentially a two-dimensional problem, requiring an understanding of the interaction of two principal stresses and strains in a membrane element. Torsion is complicated because it is a three-dimensional problem involving

Documents
Document Sharing Hub

American Concrete Institute Copyrighted Material—www.concrete.org

Full document details: ACI 445.1R-12

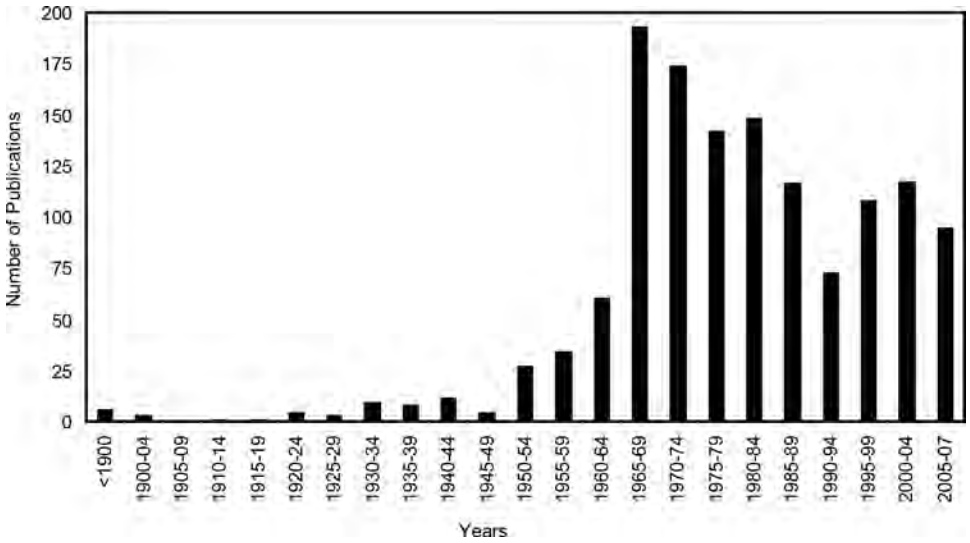


Fig. 3.3.4.2—Number of published papers on torsion from 1900 to 2007 (plot prepared by A. Belarbi).

the shear problem of membrane elements in a tube and the warping of tube walls that cause flexure in concrete struts. Figure 3.3.4.2 shows that the number of globally published papers on torsion began to surge around 1960 and peaked around 1970. The principles of equilibrium, compatibility conditions, and materials stress-strain relationships that were needed to solve torsion problems in reinforced concrete members were primarily developed between 1960 and 1985 (Lampert and Thürlimann 1971; Lampert and Collins 1972; Elfgren et al. 1974a,b; Collins and Mitchell 1980; Hsu and Mo 1983). Theories and tests produced before 1980 are summarized in detail by Hsu (1984).

By 1985, researchers solved the basic problems of reinforced concrete design by applying Navier's theory. Further research was necessary to refine the constitutive laws of materials for torsion and shear. The experimental work needed to generate new advancements is tedious and requires highly sophisticated testing equipment. Only two universities in North America—the University of Toronto and University of Houston—are capable of studying the behavior of reinforced concrete shell and panel elements subjected to in-plane shear and normal stresses. The study of softened concrete in shear elements, which has been the subject of extensive research worldwide in the last three decades, continues to be a major research topic. The need for larger and more complex specimens has increased ongoing work at both universities. The high cost of experimental research needed for new developments in torsion imposes a limiting constraint on new research. For example, studying the behavior of full-scale girders with open sections that involve Saint-Venant and warping torsion is expensive. The future of torsion research is largely tied to available equipment or to the combined efforts of many institutions, or both.

3.3.5 *Space truss model using struts and ties*—The first theory for shear design of reinforced concrete was developed at the turn of the twentieth century when Ritter (1899) and Mörsch (1902) formulated the concept of plane trusses with struts and ties. They modeled a reinforced concrete member as a truss with two types of linear elements: struts made out of concrete and ties made out of steel reinforcement. The Ritter and Mörsch model represents the struts and ties as lines without cross-sectional dimensions, where forces satisfy equilibrium at points of intersection—a model with the advantage of conceptual clarity. Extending the 2-D plane truss model to a 3-D space truss model, Rausch (1929) developed a theory for torsion of reinforced concrete. Rausch's space truss model, as shown in Fig. 3.3.5a, is made up of 45-degree diagonal concrete struts, longitudinal reinforcing bars, and hoop reinforcing bars connected at the joints by hinges. Torsional moment is carried by the concrete struts in axial compression (dotted lines), and by the straight reinforcing bars in axial tension (solid lines) in the longitudinal (horizontal) and lateral (hoop) directions. Equilibrium of the joints in the longitudinal, lateral, and radial directions requires that the forces in the longitudinal bars (X), in the hoop bars (Q), and in the inclined struts (D) should be evenly distributed among all cells and joints. To satisfy equilibrium, the relationship between these forces should be $X = Q = D/\sqrt{2}$. As shown in Fig. 3.3.5a, the series of hoop forces Q at the joints constitute a shear flow $q = Q/s$. Using Bredt's lever arm area concept, T can be related to q (or Q/s) by $2A_o$, as expressed by Bredt's equation (Eq. (3.3.3)). The term A_o refers to the area enclosed by a series of straight lines connecting joints of the cross section.

Assuming that ultimate torque is reached when the forces in the transverse reinforcement reach the yield stress, then $q = Q/s = A_t f_{ty}/s_t$ and Eq. (3.3.3) becomes

$$T_n = 2A_{oh}\frac{A_t f_{ty}}{s_t} \tag{3.3.5}$$

Although the space truss model has the advantage of conceptual clarity in terms of simple assemblage of compression struts and tension ties, Rausch's equation (Eq.

Document Sharing Hub
American Concrete Institute Copyrighted Material—www.concrete.org
Full document details: ACI 445.1R-12

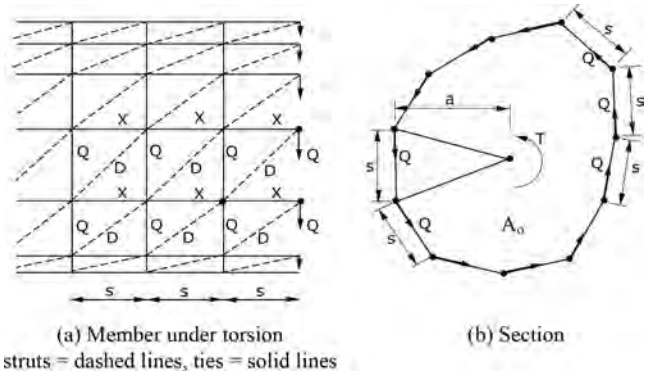


Fig. 3.3.5a—Rausch's space truss model with struts and ties (Hsu 1984 after Rausch 1929).

(3.3.5)) was found to greatly overestimate the experimentally measured torsional strengths of reinforced concrete members. As a result, empirical formulas proposed to correct limitations of Rausch's equation were incorporated in the design codes of several countries until the 1990s. Figure 3.3.5b compares T_n with $A_{oh}A_t f_{ty}/s_t$ for a series of PCA tests (Hsu 1968b,c). The straight solid line represents calculated strengths using Eq. (3.3.5) (that is, $\alpha_t = 2.0$) and the dashed line represents calculated strengths using the torsion provisions of ACI 318-71. The lever arm area A_o is defined by the centerline of closed stirrups and denoted as A_{oh}. In view of the unconservative nature of the values calculated with Eq. (3.3.5) (Fig. 3.3.5b), in particular when T_n is large, an empirical formula was proposed for ACI 318-71. This formula is simply a modification of Eq. (3.3.5), which reduced the slope of 2, shown in Fig. 3.3.5b, down to 1.2, and added a "concrete contribution T_c," which represents the vertical intercept of the experimental curve. The background of "concrete contribution T_c," which is included in early ACI Codes (1971 through 1995) and later dropped, is provided in Hsu (1997). From the experimental tests shown in Fig. 3.3.5b, Lampert and Thürlimann deduced that A_o should be less than A_{oh}. They recommended that A_o be taken as the area enclosed by a line joining the centers of the longitudinal bars in the corners of the hoops. With this change in the definition of A_o, the agreement between predictions and experimental results was considerably improved. This new definition of A_o was subsequently incorporated into the CEB-FIP code (1978). A different approach, to reconcile Rausch's space truss model with test results, was achieved in 1983 with development of the STM (Hsu and Mo 1983) for torsion, using a softened stress-strain relationship of concrete developed by Vecchio and Collins (1981). A more recent STM is provided in 5.6.

3.3.6 *Skew-bending theory for torsion*

3.3.6.1 *Beams without web reinforcement*—When beams without transverse reinforcement are subjected to torsion, they fail quickly and abruptly at cracking. Their torsional behavior is similar to that of plain concrete beams and, therefore, can be predicted by Saint-Venant's theory. The experimental torsional strength of a plain concrete beam, however, was found to be greater than the theoretical strength calcu-

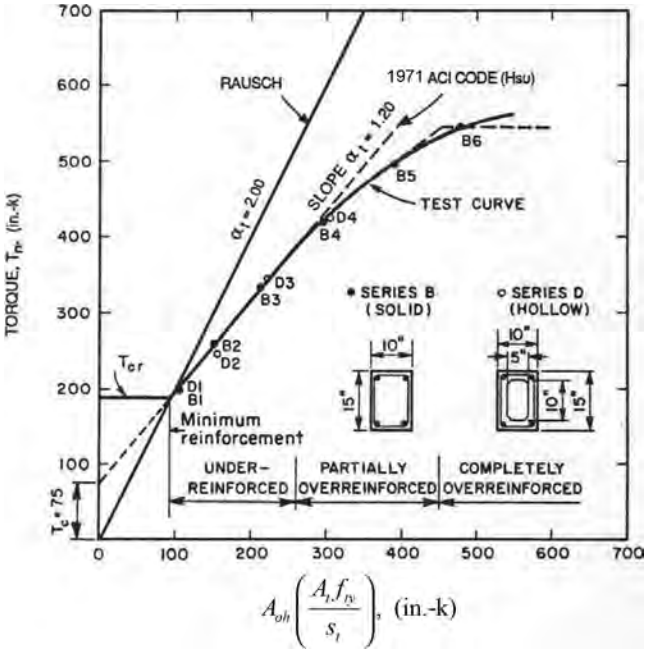


Fig. 3.3.5b—Experimental T_n *versus* $A_{oh}(A_t f_{ty}/s_t)$ *curve compared with Rausch's formula and 1971 ACI code (Hsu 1984).*

lated with Saint-Venant's theory ($T_n = \alpha x^2 y f_t'$), assuming the principal tensile stress reaches a value of f_t'. To find a reason for this discrepancy, Hsu (1968a) used high-speed photography to record failure process and observed that plain concrete members failed abruptly in a skew-bending mode. Based on the skew-bending failure, the torsional strength was derived as $T_n = (1/3)x^2 y(0.85 f_r)$. As a result, the constant 1/3 is an approximation of Saint-Venant's coefficient α when the x/y ratio becomes large. This coefficient was used as the calibration for the torsional strength of beams without reinforcement, and for the "concrete contribution" of the torsional strength of beams with web reinforcement (Hsu 1968b,c). Formulas based on the parameter $(1/3)x^2 y f_t'$ were incorporated into the ACI Code from 1971 to 1995.

3.3.6.2 *Beams with web reinforcement*—Skew-bending theory was also applied to concrete beams reinforced with both longitudinal and transverse reinforcement subjected to torsion, shear, and flexure. Such beams could fail in three modes (Fig. 3.3.6.2). The first mode has a compression zone along the top face and failure is caused by yielding of the bottom longitudinal reinforcement and transverse reinforcement along the three remaining faces. The second mode has a compression zone along a side face and failure is caused by the yielding of the longitudinal reinforcement on the opposite side face, and in the transverse reinforcement along the three faces in tension. The third mode has a compression zone along the bottom face where failure is caused by yielding along the top longitudinal reinforcement and transverse reinforcement along the three remaining faces.

Lessig (1959) was the first to propose a skew-bending theory in connection with Mode 1 and Mode 2 failures. Equilibrium equations were established by taking moments equilibrium about an axis (EF, Fig. 3.3.6.2) parallel to the

American Concrete Institute Copyrighted Material—www.concrete.org
Full document details: ACI 445.1R-12
Document Sharing Hub

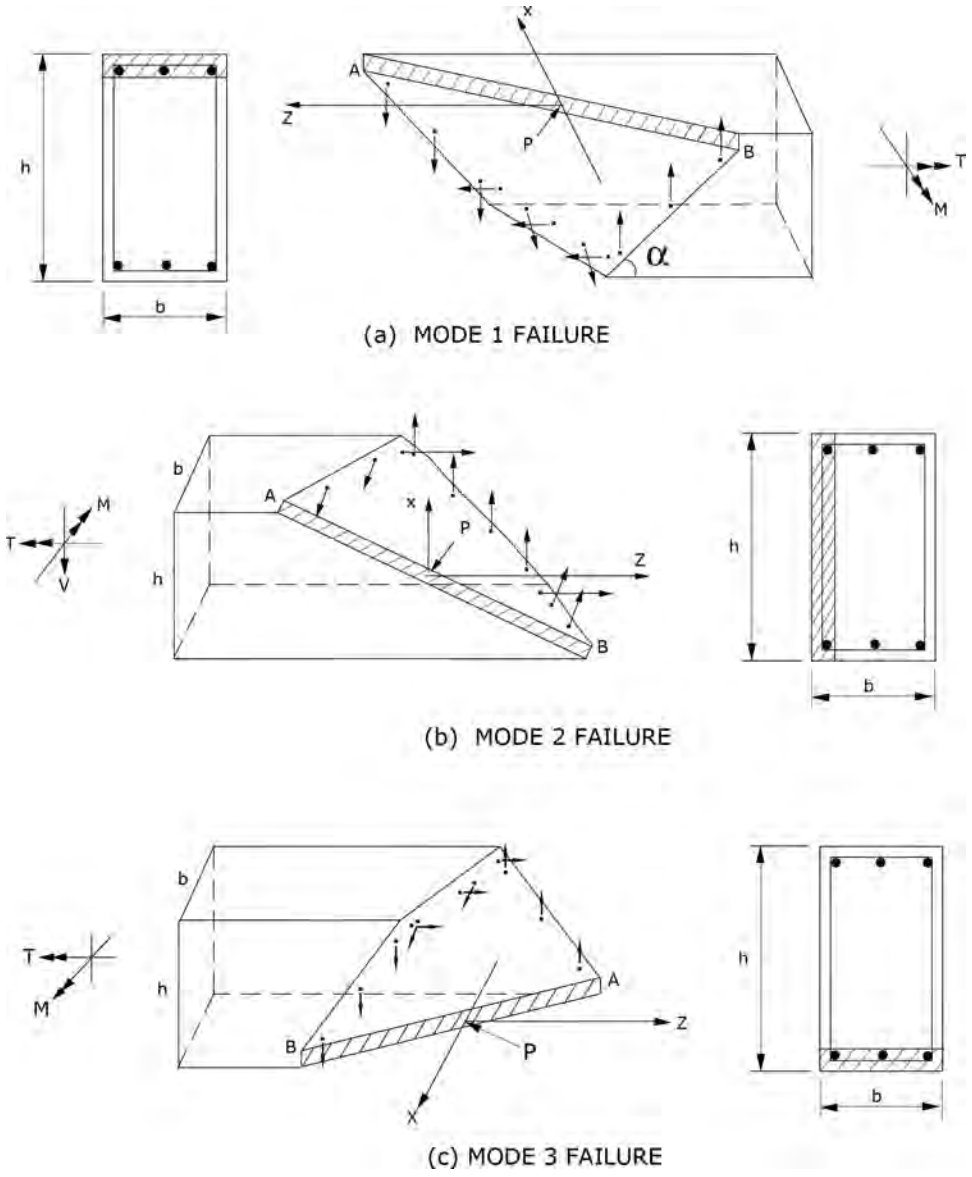


Fig. 3.3.6.2—Three failure modes in skew-bending theories (Lessig 1959; Yudin 1962; Collins et al. 1968a; Elfgren et al. 1974a,b).

skew compression zone and force equilibrium about the axis perpendicular to the center of the compression zone. The crack angles defining the skew failure surfaces were determined by minimizing the torsional resistance. The resulting equations were complicated.

Yudin (1962) took a different approach by deriving three equilibrium equations: moment equilibrium about the longitudinal and transverse axes through the compression zone center, and force equilibrium about the axis perpendicular to the compression zone center. Assuming all the crack angles to be 45 degrees, he showed that his equation for ultimate torque was the same as Rausch's. Lessig and Yudin's research was followed by the skew-bending theory of Walsh et al. (1966, 1967) and Collins et al. (1968a,b), who also identified Mode 3 failure. The three modes of failure—1, 2, and 3—are governed by the dominant effect of positive flexure moment, torsion shear, and negative flexure moment, respectively. For combined torsion and flexure, Lampert and Collins (1972) showed that both the skew-bending theory and the space truss theory predict the same parabolic shape for the interaction curve. Elfgren et al. (1974a,b) then derived a nondimensional interaction surface for combined torsion, shear, and flexure based on the three modes of skew-bending failure. If the inclination angle of cracks in each wall is adjusted so that both longitudinal and transverse reinforcement can yield, the interaction surface becomes identical to that derived from the equilibrium (plasticity) truss model (Elfgren 1972a,b), as explained in 5.5.

3.3.7 *Truss models with membrane elements*

3.3.7.1 *Equilibrium (plasticity) truss model for torsion*—Rausch's space truss model with struts and ties (1929) was replaced by a new and more realistic type of truss model in the 1960s. As shown in Fig. 3.3.7.1a, the new model is made up of membrane elements treated as trusses made up

AVA Documents Document Sharing Hub

American Concrete Institute Copyrighted Material—www.concrete.org

Full document details: ACI 445.1R-12

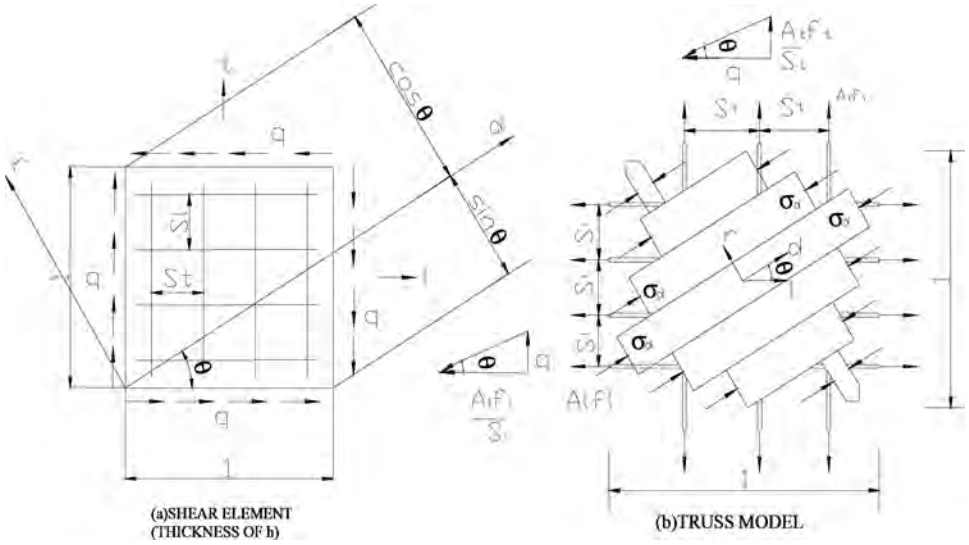


Fig. 3.3.7.1a—Membrane element in shear (Hsu 1993).

of struts and ties after cracking. Three equilibrium equations for the elements were first derived by Nielsen (1967) and Lampert and Thürlimann (1968).

$$\sigma_\ell = \sigma_d \cos^2\theta + \sigma_r \sin^2\theta + \rho_\ell f_\ell \qquad (3.3.7.1a)$$

$$\sigma_t = \sigma_d \sin^2\theta + \sigma_r \cos^2\theta + \rho_t f_t \qquad (3.3.7.1b)$$

$$\tau_{\ell t} = (-\sigma_d + \sigma_r)\sin\theta\cos\theta \qquad (3.3.7.1c)$$

Because Eq. (3.3.7.1a) through (3.3.7.1c) describe the transformation of stresses, they form a system of stresses that should satisfy Mohr's stress circle, a type of equilibrium condition called Mohr's circular stress equilibrium. The longitudinal and transverse reinforcement stresses are assumed to yield at failure ($f_\ell = f_{\ell y}$, $f_t = f_{ty}$), and the concrete tensile stress is neglected ($\sigma_r = 0$). Equations (3.3.7.1a) through (3.3.7.1c) were simplified to yield the shear stress $\tau_{\ell t}$ in the case of pure shear without normal stresses ($\sigma_\ell = \sigma_t = 0$)

$$\tau_{\ell t} = \sqrt{\rho_\ell f_{\ell y} \rho_t f_{ty}} \qquad (3.3.7.1d)$$

A reinforced concrete tube subjected to torsion can be visualized as an assembly of shear elements similar to the one shown in Fig. 3.3.3.

The torsional moment at yielding, T_n, can then be derived by substituting the shear stress $\tau_{\ell t}$ ($\tau_{\ell t} = q/t$) into Eq. (3.3.3) and substituting $\rho_\ell = A_\ell/s_\ell t$ and $\rho_t = A_t/s_t t$

$$T_u = 2A_o \sqrt{\frac{A_\ell f_{\ell y}}{s_\ell} \frac{A_t f_{ty}}{s_t}} \qquad (3.3.7.1e)$$

Equation (3.3.7.1e) was first derived by Lampert and Thürlimann (1968, 1971). In the case of equal yield force in both longitudinal and transverse reinforcement ($A_\ell f_{\ell y}/s_\ell = A_t f_{ty}/s_t$), Lampert and Thürlimann's Eq. (3.3.7.1e) looks identical to Rausch's Eq. (3.3.5), except the term A_o is defined differently. The former is based on the centerline of longitudinal reinforcement and the latter is based on the centerline of hoop reinforcement. Equation (3.3.7.1e) was first used in the European CEB-FIP code in 1978 and ACI 318-95. By combining Eq. (3.3.7.1e) with equations for shear and flexure, Elfgren (1972a,b) and Elfgren et al. (1974a) established a nondimensional interaction surface as shown in Fig. 3.3.7.1b, based on the equilibrium (plasticity) truss model as explained in 6.5. Elfgren also showed the interaction surface derived from the truss model is identical to the skew-bending theory. Actual testing has shown, however, that Elfgren's interaction surface overestimates the experimental results in the region adjacent to torsion and shear because softening concrete was not considered.

3.3.7.2 *Compatibility truss model for torsion*

3.3.7.2.1 *General*—According to Navier, the strain compatibility (or geometric) condition should be considered if the angle of twist is to be related to the torsional moment. Assuming the membrane element to behave as a truss as shown in Fig. 3.3.7.1a(b), three strain compatibility equations have been derived by Baumann (1972) and Mitchell and Collins (1974).

$$\varepsilon_\ell = \varepsilon_d \cos^2\theta + \varepsilon_r \sin^2\theta \qquad (3.7.2.1a)$$

$$\varepsilon_t = \varepsilon_d \sin^2\theta + \varepsilon_r \cos^2\theta \qquad (3.7.2.1b)$$

$$\frac{\gamma_{\ell t}}{2} = (-\varepsilon_d + \varepsilon_r)\sin\theta\cos\theta \qquad (3.7.2.1c)$$

Because Eq. (3.7.2.1a) through (3.7.2.1c) describe the transformation and distribution of strains, they should satisfy Mohr's strain circle. This type of compatibility condition is therefore called Mohr's circular strain compatibility.

American Concrete Institute Copyrighted Material—www.concrete.org

Full document details: ACI 445.1R-12

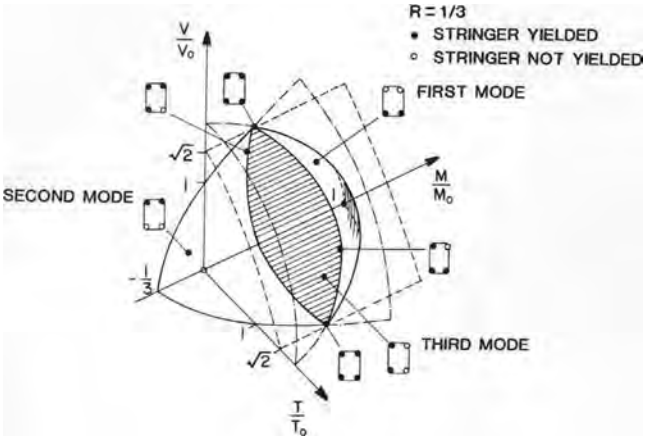


Fig. 3.3.7.1b—Nondimensional interaction surface for torsion, shear, and flexure (Hsu 1984). (The numbering of the failure modes is different than in Fig. 3.3.6.2.)

In addition, there are two compatibility equations for a reinforced concrete tube. One relates the angle of twist, Φ, to the shear strain $\gamma_{\ell t}$ of the membrane element

$$\Phi = \frac{p_o}{2A_o}\gamma_{\ell t} \qquad (3.7.2.1d)$$

The other describes the flexure of diagonal concrete struts. The curvature of concrete struts Ψ at an angle θ is related to the angle of twist Φ by

$$\Psi = \Phi \sin 2\theta \qquad (3.7.2.1e)$$

3.3.7.2.2 *Compression field theory (CFT)*—In a major development of the truss model for torsion, Mitchell and Collins (1974) established the CFT to calculate the complete torque-twist response of reinforced concrete members, irrespective of sectional shape or amount of reinforcement. The CFT combines four equilibrium equations [Eq. (3.3.3), (3.3.7.1a), (3.3.7.1b), and (3.3.7.1c)], five compatibility equations [Eq. (3.7.2.1a) through (3.7.2.1e)], and constitutive equations of concrete and reinforcement. Concrete diagonals thickness t_d and the area enclosed by the shear flow, A_o, are determined as described in 5.5. The assumption that the diagonal compressive strains are reduced linearly with depth below the surface was experimentally verified (Collins 1973). Because the concrete cover is assumed to have spalled before the section reaches the maximum strength, this theory is also known as the "spalling model." Details of the CFT are provided in 5.5.

3.3.7.2.3 *Softened truss model*—A reinforced concrete membrane element subjected to shear is a two-dimensional problem; the shear stress can be resolved into a principal tension stress and a principal compressive stress in the 45-degree direction. Robinson and Demorieux (1972) found that when a membrane element is subjected to a biaxial stress condition, the principal compressive stress is reduced (or "softened") by the principal tensile stress in the perpendicular direction. Performing biaxial tests of shear elements, Collins and Chockalingam (1979) and Vecchio and Collins (1981, 1982, 1986) showed that the concrete softening coefficient in the principal compressive direction is related to the principal tensile strain, not the principal tensile stress. Softening was further quantified experimentally by researchers at the University of Houston (Belarbi and Hsu 1994, 1995; Pang and Hsu 1995; Hsu et al. 1995a,b; Zhang and Hsu 1998), who confirmed the importance of principal tensile strain and identified concrete strength as an additional essential variable. An STM (Hsu and Mo 1985a,b,c; Hsu 1993) was developed based on a softened concrete stress-strain curve. Details of this theory are provided in 4.6. In the STM (Hsu and Mo 1985a,b,c), the softened concrete stress-strain curve is used in the flexural compression zone of the concrete struts to determine the neutral axis position. The distance from the neutral axis to the extreme compression fiber is known as thickness of shear flow zone, t_d; the lower the softening coefficient, the greater the thickness t_d. Because the softening coefficient varies from approximately 1/4 to 1/2, the thickness t_d, obtained from the softened stress-strain curve, is expected to be approximately two to four times the thickness from the non-softened stress-strain curve. Based on Vecchio and Collins's softened stress-strain curve (1981), Hsu and Mo (1985a,b,c) studied the torsional behavior of cracked reinforced concrete members. They found that Rausch's Eq. (3.3.5) is valid if the thickness t_d and the lever arm area A_o are calculated by a truss model that incorporates a softened stress-strain curve. Hsu and Mo's STM satisfies the Mohr's stress circle, the Mohr's strain circle, and the softened stress-strain curve of concrete. It was further shown to provide accurate estimates of experimental results available at the time (Hsu and Mo 1985a,b,c), including the PCA tests in Fig. 3.3.5b. When accounting for the modifications proposed by Hsu and Mo, the equation by Rausch becomes a curve that starts at the origin, closely tracing the PCA test points. This occurs because A_o decreases with increasing T_n and an increasing percentage of reinforcement. The dependency of t_d and A_o on T_n is expressed by simple equations (Hsu 1990, 1993)

$$t_d = \frac{4T_n}{A_{cp} f_c'} \qquad (3.3.7.2.3a)$$

$$A_o = A_{cp} - \frac{t_d p_o}{2} \approx A_{cp} - \frac{t_d p_{cp}}{2} = A_{cp} - \frac{2T_n p_{cp}}{A_{cp} f_c'} \qquad (3.3.7.2.3b)$$

As indicated by Eq. (3.3.7.2.3b), the lever arm area A_o is decreased by increases in the thickness t_d. Because the torsional strength of a reinforced concrete member is directly proportional to A_o, the strong effect of the softening coefficient on the torsional strength is evident, explaining why Rausch's equation for T_n (Eq. (3.3.5)) overestimated the test results, as shown in Fig. 3.3.5b. Because the shear flow zone thickness t_d occupies such a crucial position in the STM, torsion research is now focused on a better understanding of the shear flow zone (Alkhrdaji and Belarbi 2003).

Documents
Document Sharing Hub
American Concrete Institute Copyrighted Material—www.concrete.org
Full document details: ACI 445.1R-12

3.3.8 *Derivation of ACI 318: torsion design equations*—As discussed previously, ACI equations for designing members under torsion are based on the space truss model theory. There are two basic design equations: one for torsional hoop reinforcement, and another for torsional longitudinal reinforcement.

From the truss model (Fig. 3.3.7.1a(b)), equilibrium of the top face of the element relates the shear flow q to the force in the torsional hoop reinforcement per unit length ($A_t f_t/s$) through the equation

$$q = \frac{A_t f_t}{s}\cot\theta \tag{3.3.8a}$$

Substituting Eq. (3.3.8a) into Bredt's Eq. (3.3.3) and assuming yielding of the hoop reinforcement renders the ACI 318 requirement for transverse reinforcement for torsion.

$$\frac{A_t}{s} = \frac{T_u}{\phi 2A_o f_{yv}\cot\theta} \tag{3.3.8b}$$

Similarly, from the equilibrium of the left face of the element, shown in Fig. 3.3.7.1a(b), the shear flow q can be related to the force in the torsional longitudinal reinforcement per unit length ($A_\ell f_\ell/s_\ell$) through the equation

$$q = \frac{A_\ell f_\ell}{s_\ell}\tan\theta \tag{3.3.8c}$$

The term A_l is defined in ACI 318 as the total area of torsional longitudinal reinforcement in the cross section, assuming that $p_o = p_h$, where p_h is the perimeter of the centerline of the outermost hoop bars. Equation (3.3.8c) then becomes

$$q = \frac{A_\ell f_\ell}{p_h}\tan\theta \tag{3.3.8d}$$

An expression for the amount of torsional longitudinal reinforcement in ACI 318 is obtained by equating the shear flow q of Eq. (3.3.8d) and (3.3.8a)

$$A_\ell = \left(\frac{A_t}{s}\right) p_h \frac{f_{yv}}{f_{y\ell}}\cot^2\theta \tag{3.3.8e}$$

3.4—Concluding remarks

This historical review identifies research studies that have provided the foundation for the current understanding of torsion in reinforced concrete members. It took almost the entire twentieth century for researchers to successfully apply Navier's theory to cracked reinforced concrete. The application of Navier's theory to the flexure theory of reinforced concrete was relatively easy because of the one-dimensional condition of equilibrium and compatibility, combined with the non-softened constitutive laws of materials. Shear and torsion proved to be much more difficult because they were, respectively, two-dimensional and three-dimensional problems. From a historical perspective, the development of the current torsional theories spanned over 40 years. Equilibrium equations were developed in the 1960s, compatibility conditions were added in the 1970s, and the formulation and expressions of softening coefficients were introduced in the 1980s and 90s.

Since 1960, the bulk of work has focused on beams subjected to monotonic torsional loading. Early tests on members subjected to reverse cyclic loading were conducted by Collins and Chockalingam (1979) on reinforced concrete beams subjected to pure torsion and by Stevens et al. (1991) on membrane elements subjected to reversed cyclic shear up to reinforcement yielding. Significant recent advances have applied rational models such as the STM and the modified CFT to shear elements subjected to cyclic loading. Vecchio (1999) and Palermo and Vecchio (2003, 2004) applied the MCFT for cyclic loading up to yielding of the reinforcement. Mansour et al. (2001), Zhu et al. (2001), Zhu and Hsu (2002), and Mansour and Hsu (2005a,b) studied cyclic torsion and shear, including the unloading and reloading branches of the softened stress-strain curves (hysteretic loop) and the effect of Poisson's ratio in a membrane element. The latter was crucial in determining the descending branch of the softened stress-strain curve.

Belarbi and Greene tested several full-scale box girders under cyclic torsion and combined torsion and shear (Belarbi and Greene 2004; Greene and Belarbi 2008). The cyclic shear tests of membrane elements (Mansour and Hsu 2005a,b) permitted the establishment of cyclic stress-strain curves of concrete and reinforcement. These cyclic constitutive laws laid the foundation for the Cyclic Softened Membrane Model (Mansour and Hsu 2005a,b), which could be used for the design of seismic-resistant reinforced concrete structures (Hsu et al. 2006).

CHAPTER 4—BEHAVIOR OF MEMBERS SUBJECTED TO PURE TORSION

4.1—General

The torsional strength of concrete beams depends on many factors, such as the amount and distribution of transverse and longitudinal reinforcement, concrete strength, cross section shape, and, for rectangular cross sections, aspect ratio (depth-to-width ratio). Concrete strength and amount of reinforcement can change the failure characteristics. The failure mechanism varies from ductile to sudden and brittle, depending on the longitudinal and transverse reinforcement volumetric ratios. Chapter 4 details the behavior of plain concrete, reinforced concrete, and prestressed concrete under pure torsion. The behavior of high-strength concrete members is also discussed. The effects of other stress resultants, such as shear and flexure, are discussed in Chapter 6.

4.2—Plain concrete

Saint-Venant's elastic theory accurately describes the torsional behavior of plain concrete members at low torque before cracking. This theory assumes that the cross section

Document Sharing Hub

American Concrete Institute Copyrighted Material—www.concrete.org

Full document details: ACI 445.1R-12

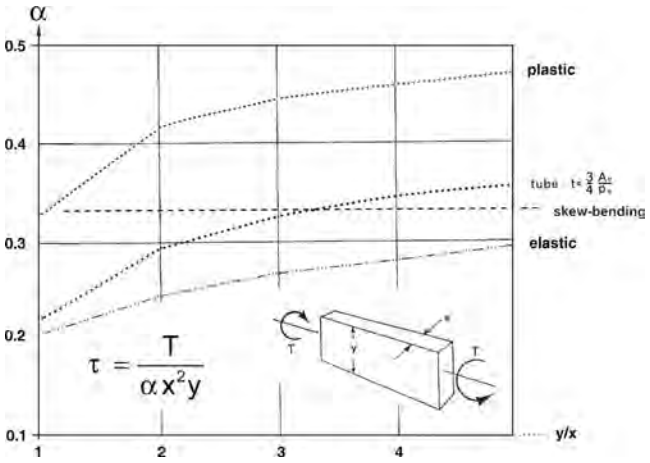


Fig. 4.2—Torsion stress factors for solid rectangular section (Collins 1973).

shape remains unchanged after twisting, the angle of twist per unit length is constant along the element length, warping deformation perpendicular to the cross section is identical throughout the member length, and failure occurs when the maximum principal stress equals the direct concrete tensile strength. Member shear stresses resist applied torsional moment. For solid circular shapes, the shear stresses are zero at the member center, increasing linearly to a maximum at the outside surface. In solid rectangular shapes, the shear stresses increase from zero at the center to a maximum at the center of the longer faces, but they decrease along the edge and are zero again at the corners. When considering a small element in the member subjected to pure torsion, only shear stresses develop and, therefore, the principal tension and compression stresses equal the shear stress. Applying Saint-Venant's theory to concrete, the member would fail in a brittle manner once the maximum shear stress equals the concrete tensile cracking strength.

After cracking, the elastic theory does not accurately describe the concrete behavior because various nonlinearities exist, such as the stress-strain behavior in compression, post-peak softening in tension, and tensile cracking. When the elastic theory is used, it considerably underestimates the torque at failure of a plain concrete member because concrete exhibits a complex structural response (Hsu 1984; Karayannis 2000). Other theories, such as the plastic theory and skew-bending theory, were developed to estimate the failure strength of plain concrete members. The plastic theory is not theoretically satisfactory because it assumes that concrete develops plasticity. As in the elastic theory, failure is assumed to occur when the maximum principal tensile stress of concrete reaches the tensile strength. Concrete, however, does not develop significant plastic behavior in tension and the torsional failure of plain concrete is brittle (Hsu 1984). Unlike the elastic theory, the plastic theory tends to overestimate the failure strength. The skew-bending theory assumes that plain concrete members subjected to torsion fail by bending about an axis parallel to the wider cross-sectional face and inclined at an angle of 45 degrees with respect to the longitudinal axis. Failure occurs when the tensile stress on the inclined face due to flexure reaches a reduced modulus of rupture of concrete (Hsu 1968b). The formula derived is $T_u = (1/3)x^2y(0.85f_r)$. The torsional stress factor is a constant 1/3, which lies between those of the elastic theory and the plastic theory, as shown in Fig. 4.2. The skew-bending theory accurately describes the failure of concrete elements with rectangular cross sections, but it should be considered as an assembly of component rectangles when applied to flanged sections (Hsu 1968b, 1984). For thin-walled tubes, the relationship between torsional shear stress τ (= q/t_d) and the torsional moment T can be found from Bredt's Eq. (4.2). Collins (1973) suggested that if a solid section was replaced by a tube with the same exterior dimensions but with a wall thickness of $0.75A_o/p_o$, the cracking torques could still be determined from Eq. (4.2). Figure 4.2 compares the torsional shear stress τ for solid rectangular sections predicted by elastic theory, plastic theory, skew-bending, and thin-walled tube model. By further assuming that the wall thickness $t_d = 0.75A_{cp}/p_{cp}$ and that $A_o = (2/3)A_{cp}$, the torsional stress τ can be related to T by the parameter (A_{cp}^2/p_{cp})

$$\tau = \frac{T}{2A_o t_d} = \frac{T}{(A_{cp}^2 / p_{cp})} \tag{4.2}$$

Equation (4.2) was embraced by CSA-A23.3-77 and later adopted by ACI 318-95. For example, the ACI code uses it to address compatibility torsion of spandrel beams. When the nominal torsional stress τ_n needed to form a torsional plastic hinge was found to be $0.33\sqrt{f_c'}$ MPa ($4\sqrt{f_c'}$ psi) (Hsu and Burton 1974; Hsu and Hwang 1977), the design torsional moment T_n of the spandrel beam was $0.33\sqrt{f_c'}\,(A_{cp}^2/p_{cp})$ MPa (equivalent to $4\sqrt{f_c'}\,(A_{cp}^2/p_{cp})$ psi).

In addition to the aforementioned theories, there are approaches to the torsional behavior of concrete elements that are based on truss models. Because these models are developed on modeling the flow of forces in a cracked reinforced concrete element, as stated by Karayannis (1995), these approaches are more suitable for the description of the post-elastic behavior of reinforced concrete elements, with rectangular cross sections reinforced in the longitudinal and transverse directions.

Karayannis and Chalioris (2000) confirmed that a plain concrete member subjected to pure torsion fails in tension due to shear. The behavior of concrete elements in torsion is therefore primarily governed by the material tensile response, particularly its tensile cracking characteristics. Tension cracking makes the plain concrete behavior in torsion nonlinear. Before the peak torque is reached, some microcracking and softening regions are developed.

The cracking is a localized phenomenon, and its boundary is the strain softening region called the fracture process zone. Bažant and Oh (1983) regarded this tension-softening region as being caused not only by microcracking but also by bond rupture; therefore, the fracture process zone has to be assumed wider than the region of visible microcracks. The zone width can be considered as a material property that, except for the influence of the stress distribution, depends

Documents Document Sharing Hub

American Concrete Institute Copyrighted Material—www.concrete.org

Full document details: ACI 445.1R-12

on the nature and size of the aggregate. The role of the size effect on the fracture process zone width should also be considered. Between the microcracks of this zone, there are less damaged or even elastic parts; this can be considered a result of the strong tendency for eventual localization of the damage and the simultaneous recovery of the undamaged or less-damaged parts between the final cracks.

4.3—Reinforced concrete

Before the concrete cracks, a member under pure torsion is assumed to behave elastically with a nearly linear torque-twist curve. After cracking, the resistance mechanism changes and stirrups and longitudinal reinforcement carry most of the tensile load whereas the concrete carries the compression. The longitudinal reinforcement tensile strains cause the member to lengthen. Increased torque causes a nearly linear increase in the beam length. A longitudinal restraint acts as a compressive prestress force and increases the torsional strength.

Members reinforced for torsion typically have closed stirrups and at least one longitudinal bar in each stirrup corner, as originally required in ACI 318-63. Members with only longitudinal reinforcement behave similarly to a plain concrete member in regards to torsional rigidity and torsional strength, and they fail after cracking in a brittle manner. An uncracked beam loaded in pure torsion has only shear stresses on a plane perpendicular to the longitudinal axis. The associated principal tensile stress causes inclined cracks on the beam surface in the principal compressive stress direction. These cracks spiral around the beam. The tensile cracks are due to strain in the principal tensile stress direction, and they affect the concrete acting in compression. The tensile strains have the effect of weakening the concrete's ability to withstand compression in the perpendicular direction. This is known as "softening" of the concrete compressive strength. Tests performed by Vecchio and Collins (1982, 1986) identified the principal tensile strains as the primary variable influencing tension softening and quantified them. Continued work by Belarbi and Hsu (1994, 1995), Pang and Hsu (1995), Hsu and Zhang (1997), Hsu and Zhu (2002), and Hsu and Mo (2010) has improved the understanding of compression softening. Other studies, such as those of Vecchio and Collins (1993) and Koutchoukali and Belarbi (2001), have also been reported based on further calibration of their original models. After cracking, the longitudinal and transverse reinforcement are in tension, and the concrete struts between the diagonal cracks are in compression, as shown in Fig. 4.3a. The faces of the beam are warped as the beam is twisted, causing bending stresses, in addition to compressive stresses, in the concrete struts (Mitchell and Collins 1974). The concrete between inclined cracks is capable of acting in tension and will increase the overall beam torsional stiffness. This effect, known as tension stiffening, is most predominant immediately after the first cracks appear and decreases with increased torsion.

The volumetric ratios ρ_l and ρ_t have a significant effect on the behavior of reinforced concrete beams subject to pure torsion. The ratios affect the angle of the inclined cracks on the surface, crack width, beam strength and stiffness, and failure mode. The reinforcement ratios have a strong influence on the inclined crack angles and the size of the cracks. The crack width is related to the principal tensile strain. When the volumetric ratios ρ_ℓ and ρ_t are equal, θ is approximately 45 degrees and the cracks have the smallest width because the strains in the longitudinal and transverse directions are also equal. For beams with ρ_t larger than ρ_ℓ, the angle is greater than 45 degrees relative to the horizontal and the strain larger in the longitudinal direction, which causes wider cracks. Similarly, in beams with ρ_t less than ρ_ℓ, the angle is less than 45 degrees relative to the horizontal, the transverse strain is larger, and the cracks are also wider than when θ is 45 degrees (Mitchell and Collins 1974; Hsu 1993).

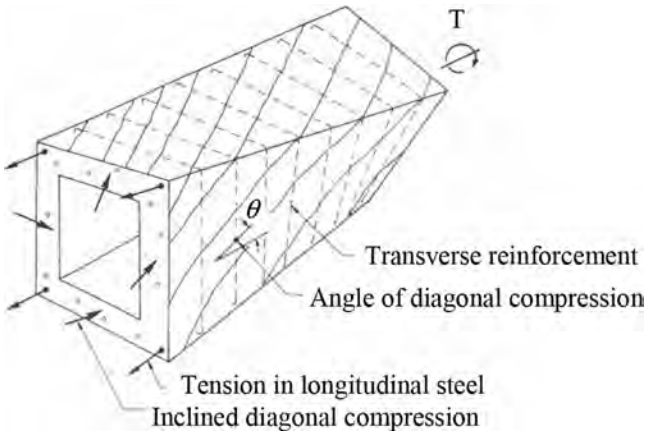


Fig. 4.3a—Diagonal cracks in members under pure torsion (Mitchell and Collins 1974).

The volumetric ratios of longitudinal and transverse reinforcement to concrete affect the failure mechanism. Large ρ_ℓ and ρ_t result in reinforcement stresses less than yield when the concrete reaches its ultimate compressive strain at the surface. In this condition, the concrete is crushed and the beam experiences sudden and brittle failure. Beams of this type are called over-reinforced. Figure 4.3b shows an example of beam failure boundaries (Leu and Lee 2000). The condition known as balanced failure point is met when concrete reaches its ultimate strain at the point where both transverse and longitudinal reinforcement begin to yield simultaneously. Beams with ρ_ℓ and ρ_t less than the reinforcement ratios at the balanced condition are called under-reinforced (Region I). Under-reinforced beams are capable of continued twist as the reinforcement yields, producing a ductile failure. Over-reinforced beams are in Region IV where the failure is brittle. For lower ratios of either ρ_ℓ or ρ_t, the longitudinal or transverse reinforcement yields before the concrete is crushed. Beams of this type are called partially under-reinforced (Regions II and III).

The volumetric ratios of longitudinal and transverse reinforcement have a strong influence on the beam's postcracking torsional stiffness and strength as shown in Fig. 4.3c. For under-reinforced beams with equal volumetric ratios ρ_l and ρ_t, an increase in the total reinforcement increases the torsional rigidity, which is the slope of the torque-twist curve

Document Sharing Hub
American Concrete Institute Copyrighted Material—www.concrete.org
Full document details: ACI 445.1R-12

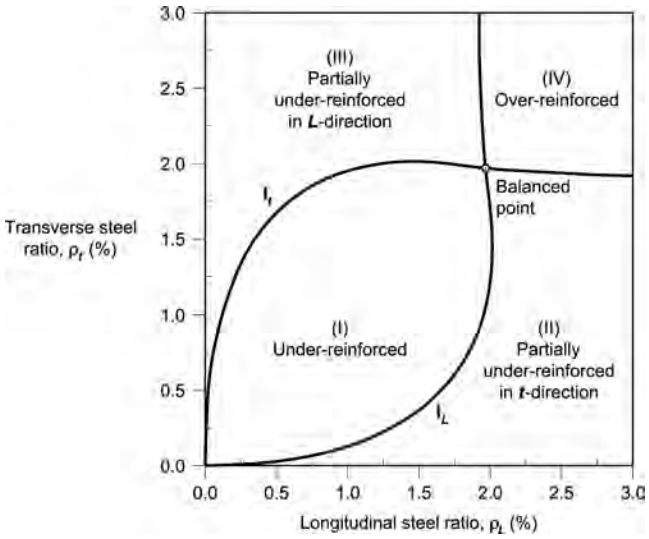


Fig. 4.3b—Failure boundaries for f_c' = 4.0 ksi (27.5 MPa) and f_y = 45.2 ksi (311.9) MPa (Leu and Lee 2000).

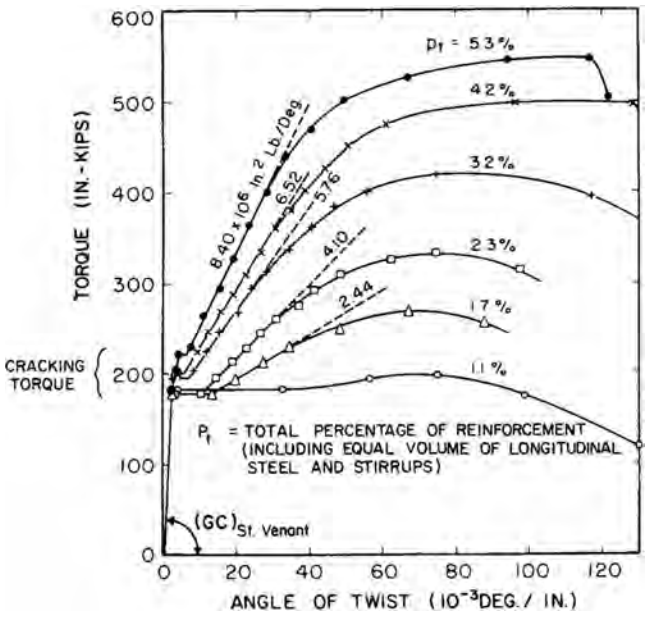


Fig. 4.3c—Torque-twist curves of beams with various percentages of reinforcement (Hsu 1968a). (Note: 1 in.-kip = 0.113 kN·m; 1 in. = 0.0254 m.)

after cracking. It also increases the torsional yield strength, which is the amount of torque the beam can sustain at the onset of yielding. As the total amount of reinforcement increases, however, the post-yield twist decreases. Therefore, an increase in the total amount of reinforcement results in a stiffer and stronger beam, but at the cost of decreased ductility. The minimum amount of reinforcing steel is the amount causing the reinforcement to yield at the same torque that causes cracking. Where this occurs, the total reinforcement ratio, including both longitudinal and transverse reinforcement, is approximately 0.01 for normal-strength concrete (Hsu 1984). A beam with less reinforcement than the minimum fails in a brittle manner after cracking. The behavior of solid members compared with hollow ones

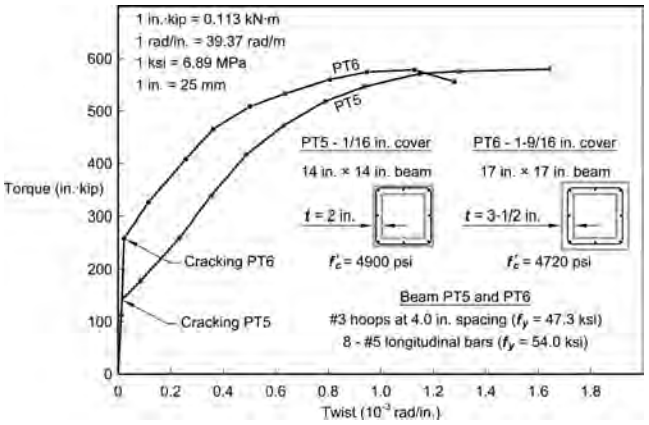


Fig. 4.3d—Effects of concrete cover on the torque-twist behavior (Mitchell and Collins 1974). (Note: 1 in.-kip = 0.113 kN·m.)

shows that the inner core of solid members is not effective after cracking. The cracking strength of hollow members is less than that of solid members because, before cracking, the shearing stresses are acting over the entire section including the inner core. After cracking, however, the outer perimeter of the cross section resists the larger part of the torque with minimum contribution from the inside core; torsional strength and general behavior are similar in solid and hollow sections after cracking as long as wall thickness is large enough to accommodate the shear flow zone (Hsu 1968a). Leonhardt and Schelling (1974) confirmed these findings when they performed an extensive test series on beams in pure torsion where they systematically varied the cross section type, including rectangular with different aspect ratios, circular, and hollow box, T-shaped, and inverted L-shaped beams. They made two observations: 1) the importance of detailing by properly anchoring the stirrups and using small stirrup spacings; and 2) the importance of softening concrete in the inclined struts.

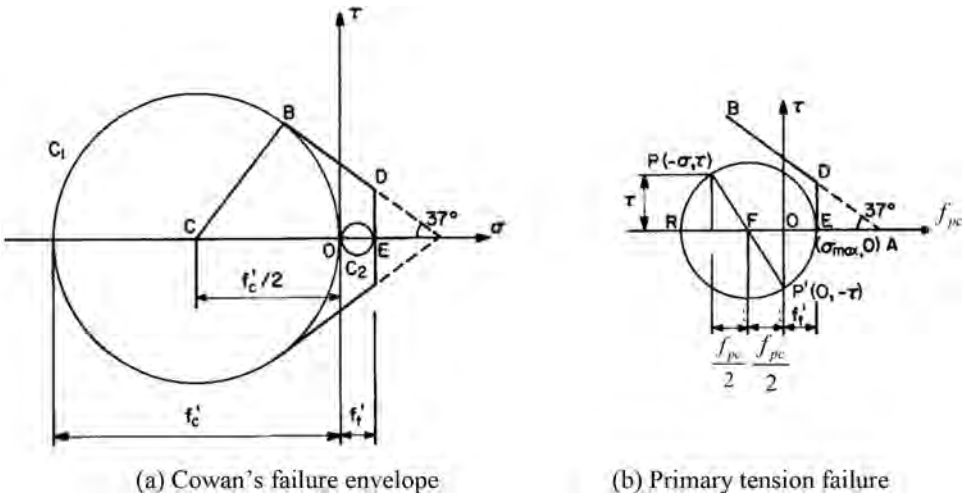
High concrete shearing stresses outside of the stirrups create potential for concrete spalling under high torques. To satisfy equilibrium, the concrete compressive stress that resists torsion after cracking changes directions at the outside corners of the beam. The resultant tensile stress in the concrete causes the concrete cover to spall off when the tensile stress is high enough. Typically the spall occurs at the stirrups. The resulting section is smaller and has a reduced torsional strength (Mitchell and Collins 1974). Mitchell and Collins (1974) tested two beams, PT5 and PT6, to investigate the effects of spalling. The beams had similar reinforcing cages and concrete strength, but PT5 had a cover of 1.5 mm (1/16 in.) and PT6 had a cover of 40 mm (1-9/16 in.). The results of the tests showed that, although the concrete outside the hoop reinforcement had a significant effect on the cracking torque, it had little effect on the peak torque after significant spalling occurred (Fig. 4.3d).

In tests performed by Rahal and Collins (1995b), specimens with small covers did not experience spalling until after the torsional strength had been reached. Beams with larger covers spalled before reaching the torsional strength.

Documents
Document Sharing Hub

American Concrete Institute Copyrighted Material—www.concrete.org

Full document details: ACI 445.1R-12



(a) Cowan's failure envelope (b) Primary tension failure

Fig. 4.4a—Cowan's failure criteria (Hsu 1984).

In these tests, the beams had stirrup dimensions of 245 x 545 mm (9.65 x 21.5 in.), and cover thicknesses of 22.5 and 42.5 mm (0.89 and 1.637 in.) for the thin and thick concrete covers, respectively. The concrete cover thickness is the critical parameter for spalling. Experiments have shown that spalling occurs if the cover thickness is greater than 30 percent of the ratio of area to the perimeter of the cross section. For this calculation, the sectional area and perimeter do not consider the area removed by voids in hollow sections (Rahal and Collins 1996).

4.4—Prestressed concrete

Adding longitudinal prestressing to a concrete member subjected to torsion will increase its cracking torque and, to a lesser extent, its failure torque. The longitudinal prestressing force creates a compression-shear biaxial state of stress that delays cracking of concrete. This effect is illustrated by Cowan's failure criteria, shown in Fig. 4.4a. The Mohr-Coulomb failure criterion has been simplified into two straight lines in Fig. 4.4a(a). If the Mohr circle of stresses touches the straight line BD described by $t = c - \tan\varphi$, where φ is the friction angle (a typical value for concrete is 37 degrees), failure is by sliding. If the Mohr circle touches the tension cutoff line DE described by $\sigma = f_t'$, failure is by separation. In Fig. 4.4a(b), $\sigma_{max} = OE = FE - FO = FP - FO$. The variable σ_{max} can then be expressed as

$$\sigma_{max} = \sqrt{\left(\frac{f_{pc}}{2}\right)^2 + \tau^2} - \frac{f_{pc}}{2} \quad (4.4a)$$

$$\tau = f_t' \sqrt{1 + \frac{f_{pc}}{f_t'}} \quad (4.4b)$$

Cowan's failure envelope using Mohr's circle is a simple and concise model for explaining the compression-shear state of stress. Equation (4.4b) for shear stress is derived from the geometry of Cowan's failure envelope, and it is a function of only the prestress and the concrete tensile strength. In effect, the longitudinal prestress increases the cracking strength, as shown in Fig. 4.4b. Expressions for prestressed member torsional strength are similar to those of reinforced concrete members with a factor that increases the strength due to the prestress. Pure torsion tests have shown that the prestressed beams appear to require approximately the same minimum torsional reinforcement as the nonprestressed beams (Hsu 1984). Similar to beams without prestressing, prestressed beams without web reinforcement fail shortly after cracking.

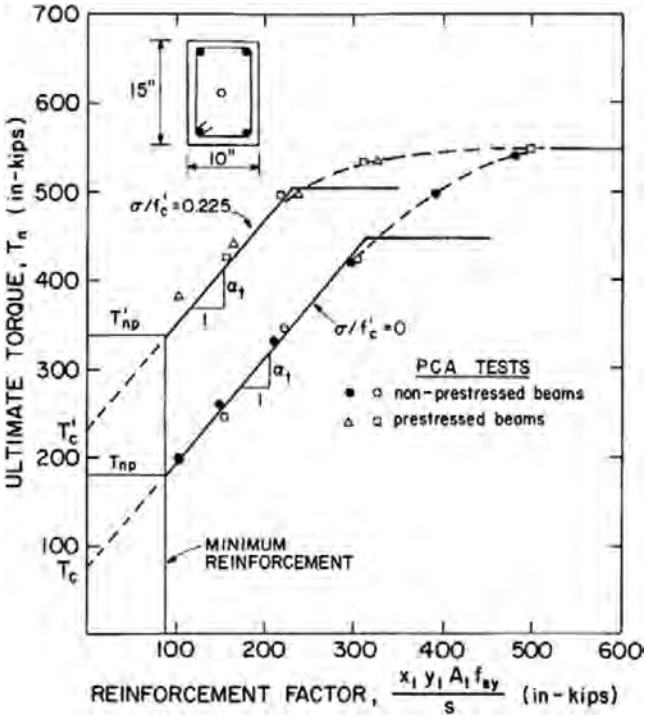


Fig. 4.4b—Ultimate torque-versus-reinforcement factor for prestressed and reinforced beams under pure torsion (Hsu 1984). (Note: 1 in.-kip = 0.113 kN·m.)

Testing has shown that as the amount of longitudinal reinforcement and prestress increase, the torque at cracking,

Document Sharing Hub
American Concrete Institute Copyrighted Material—www.concrete.org
Full document details: ACI 445.1R-12

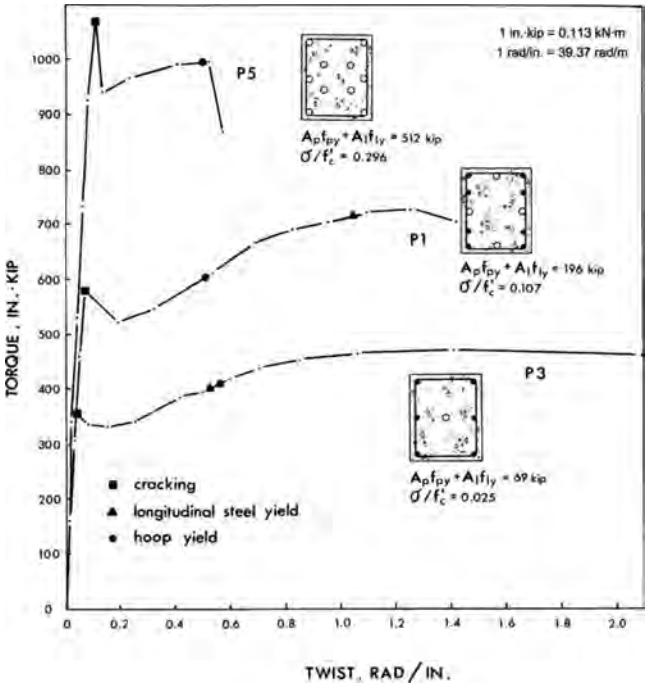


Fig. 4.4c—Effect of longitudinal reinforcement (Mitchell and Collins 1978). (Note: 1 in.-kip = 0.113 kN·m; 1 in. = 0.0254 m.)

hoop yield, and ultimate increase, whereas the twist at failure decreases. This effect is illustrated by the experimental work shown in Fig. 4.4c (Mitchell and Collins 1978). Prestressing does not influence ultimate torsional strength if the longitudinal reinforcement does not yield before failure, as shown in Specimen P5 of Fig. 4.4c. Prestressed beams under sustained, long-term torque exhibit increased rotation due to concrete creep. Beams tested to failure after being subjected to sustained torque showed no reduction in strength or stiffness. After a sustained torque, the ratio of beam rotation to the instantaneous rotation increases with larger values of torque and decreases with increased amounts of transverse reinforcement (Allos and Rashid 1989).

4.5—High-strength concrete

High-strength concrete (HSC) is more brittle than normal-strength concrete (NSC). In some ways, NSC can be treated as a perfectly plastic material, whereas HSC very much resembles a perfect elastic and brittle material (Rasmussen and Baker 1995; Iravani 1996; ACI Committee 363 1992). The ascending portion of the stress-strain curve is steep and approximately linear, whereas the descending curve almost vanishes and shows no strain softening. High-strength concrete has a peak load strain that is higher than the typical 0.0020 of NSC and an ultimate load strain less than the typical 0.0035 (Wafa et al. 1995).

In the case of pure torsion, the use of HSC allows a higher service stress in the reinforcing bars and produces a higher stiffness in the structure, enhancing both the strength and stiffness of a member. For a given amount of reinforcement, the initial crack width is larger for HSC because larger reinforcement strains are induced at cracking, but the number of cracks is fewer in HSC. Wider cracks in HSC could also be the result of reduced aggregate interlock. Shortly after the longitudinal reinforcement yield, the width of the largest crack increases rapidly. After this point, all further deformation occurs at this crack. This behavior is exaggerated in high-strength beams due to the smooth-faced cracks that are less effective in transmitting shear (Koutchoukali and Belarbi 2001). Rasmussen and Baker (1995) observed diagonal cracks in both NSC and HSC beams on the larger faces of the cross section because the shear stresses are largest on these faces. This is similar to the assumptions of the elastic theory. After first cracking, the number of cracks parallel to the initial cracks increases as the applied torque increases. In this way, characteristic spiral cracks develop around the beam. Cracking of an HSC beam is more brittle than that of an NSC beam because in HSC, not only the matrix but also the aggregate splits (the paste in HSC is strengthened relative to the aggregate), producing a more brittle response. That is, cracks in NSC matrix propagate around the aggregate, whereas cracks in HSC also pass through the aggregate. Before cracking, surface compressive principal strains for HSC beams are smaller compared with those of NSC beams because of the higher elastic modulus for HSC. Whereas HSC delays beam cracking, after cracking the shape and angle of inclination of cracks are the same for all concrete strengths (Rasmussen and Baker 1995). An HSC beam has a higher torsional stiffness than an NSC beam for a given torque and a given cross section because of the higher modulus of elasticity for HSC. Figure 4.5 shows the torque-twist diagrams for an NSC (36.3 MPa [5.1 ksi]) beam and an HSC (109.8 MPa [15.9 ksi]) beam under pure torsion, reported by Rasmussen and Baker (1995). They showed that the torque-twist curves are linear in the uncracked range and the HSC beam has greater torsional stiffness. After cracking, the torsional stiffness is reduced significantly in both beams. The post-cracking stiffness of an HSC beam remains almost linear up to failure, whereas the NSC beam curve is nonlinear.

The surface compression strain at failure for an HSC beam is slightly less than that for an NSC beam, but because of the higher modulus of rupture and consequent higher torsional stiffness for HSC, the twist at peak torque for both NSC and HSC beams is approximately the same (Rasmussen and Baker 1995). The increase in both longitudinal and transverse reinforcement stresses immediately after cracking is larger for an HSC beam than an NSC beam, resulting in brittle cracking of HSC. For the same torque, the reinforcement stresses in an HSC beam are less than in an NSC beam. Therefore, for a given torque, the required amount of beam reinforcement is less using HSC. A general comparison of the ratio of transverse reinforcement stresses and longitudinal reinforcement stresses at failure shows that this ratio increases when concrete strength increases. For HSC, the bond between concrete and reinforcement is better due to denser concrete. Therefore, the vertical component of diagonal concrete compression is easily transferred to the transverse reinforcement so that it attracts a relatively larger amount of torque using HSC. The lower bond between the

Documents
Document Sharing Hub

American Concrete Institute Copyrighted Material—www.concrete.org

Full document details: ACI 445.1R-12

stirrup and concrete using NSC results in a portion of the vertical component of the diagonal concrete compression being carried by longitudinal reinforcement bending and shear (Rasmussen and Baker 1995). Beams elongate because of increased cracking state under increasing torque. The longitudinal strains at failure increase as concrete strength increases. For the beams tested by Rasmussen and Baker (1995), the longitudinal elongation at failure for the HSC beam (B110.1) was approximately 35 percent larger than for the NSC beam (B30.3). For a given torque and given cross section, however, the longitudinal elongation of an HSC beam was approximately 50 percent lower than that of an NSC beam. Accounting for the spalling effect is essential for a correct evaluation of the ultimate torque and failure mechanism of over-reinforced HSC beams. In the case of some over-reinforced NSC concrete beams, the phenomenon of spalling does not take place, and the torsional strength is evaluated considering the entire cross section. In the case of over-reinforced HSC beams, the cover is reasonably neglected. In fact, due to the higher load-carrying strength of HSC with respect to NSC, spalling of the concrete cover from the stirrups appears to occur more frequently (Cerioni et al. 1998). This is because, even though HSC is stronger, the tensile strength does not increase in the same proportion as the compressive strength. Based on the results of 14 HSC prestressed beams tested under pure torsion, Wafa et al. (1995) concluded that increasing the concrete strength and the prestressing force increases the cracking strength, ultimate torsional strength, and torsional stiffness. Wafa et al. reported that among the several models used—the space truss model with softening of concrete (Hsu and Mo 1985a), space truss model with spalling of concrete cover (Mitchell and Collins 1974), and skew-bending theory (Hsu 1984)—the space truss theory with softening of concrete gave the best estimate of the test beams' torsional strength. Wafa et al. (1995) observed that the tensile strength increase is not in direct proportion to the compressive strength. The ratios of the modulus of rupture to the compressive strength were 9 percent and 11.4 percent, respectively, for the HSC and NSC.

The post-cracking torsional stiffness, as represented by the slope of the torque-twist curve, is influenced by the concrete strength, the amount of torsional reinforcement, and the aspect ratio. The higher the concrete compressive strength, the higher the stiffness is, irrespective of the aspect ratio and the prestressing force. Torsional strength increases with an increase in concrete strength and prestressing level and with a decrease in aspect ratio. All tested beams exhibited compression zones located on the longer sides of the beams. Tension cracks initially formed on one longer face and progressed to form spirals. Crushing on the other longer face characterized the failure pattern.

4.6—Concluding remarks

Saint-Venant's elastic theory accurately describes plain concrete members' torsional behavior at low torque and before cracking. Applying Saint-Venant's theory to concrete, the plain concrete member fails in a brittle manner once the maximum shear stress equals the concrete tensile cracking strength. For reinforced concrete members, because the elastic theory does not accurately describe the member behavior after cracking, other theories such as truss model and skew-bending were developed to estimate the failure strength.

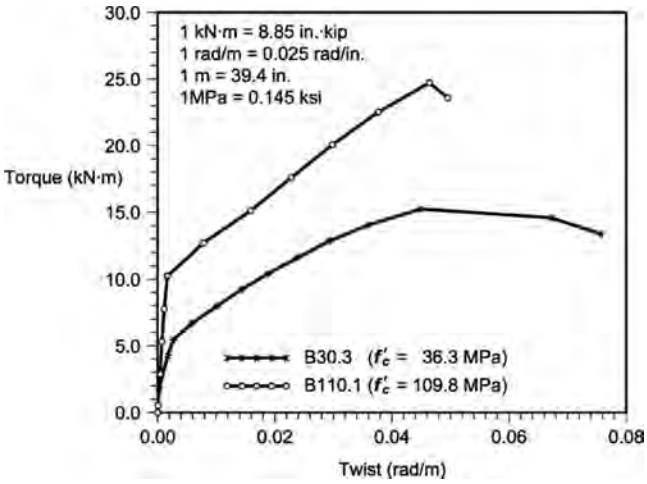


Fig. 4.5—Torque-twist relation for NSC and HSC beams (Rasmussen and Baker 1995). (Note: 1 m = 39.4 in., 1 kN·m= 8.85 in.-kip; 1 MPa = 0.145 ksi.)

In members with mild reinforcement, the longitudinal and transverse reinforcement are in tension after cracking and the concrete struts between diagonal cracks are in compression. The beam faces are warped as the beam is twisted, causing bending and compressive stresses in the concrete strut. The total amount and the relative amount of longitudinal and transverse steel reinforcement have a significant effect on the behavior of reinforced beams subject to pure torsion. The behavior of solid members compared with hollow ones shows the inner core of solid members is ineffective after cracking, making the cracking strength of hollow members less than solid ones. Torsional strength and general behavior, however, are similar in solid and hollow sections. The most significant effect of adding longitudinal prestressing to a concrete member subjected to torsion is the increase in its cracking strength. Testing has shown that as the amount of longitudinal reinforcement and the prestress force increase, the torque at cracking, hoop yield, and ultimate strength all increase whereas the twist at failure decreases. The use of HSC in torsional members allows a higher service stress in the reinforcing bars and produces a higher sectional stiffness in the structure. Cracking of an HSC beam is more brittle than that of an NSC beam; in HSC, both the matrix and aggregate split, producing a more brittle response. An increase in twist immediately after cracking is more significant for HSC beams because of the higher energy released, with more brittle crushing as concrete strength increases. The post-cracking stiffness of an HSC beam remains almost linear up to failure, whereas the curve for an NSC beam is nonlinear.

Documents
Document Sharing Hub
American Concrete Institute Copyrighted Material—www.concrete.org
Full document details: ACI 445.1R-12

CHAPTER 5—ANALYTICAL MODELS FOR PURE TORSION

5.1—General

In 1929, using space truss concepts, Rausch developed an analytical model to predict the torsional strength of reinforced concrete members. Unfortunately, Rausch's equation was unconservative by more than 30 percent for underreinforced beams (Hsu 1968a,b). Although Rausch's model assumed the lever arm area A_o to be the area within the hoop reinforcement centerline, A_{oh}, the actual A_o would be much smaller in members with a high percentage of reinforcement when concrete softening is considered. The correct determination of the lever arm area A_o and the centerline of shear flow depend on the means used to determine the thickness of the shear flow zone, t_d.

Since the late 1960s, the truss model theory has undergone four major developments. First, Lampert and Thürlimann (1968, 1969) introduced the variable angle truss model and discovered the bending phenomenon in diagonal concrete struts. Second, Collins (1973) derived compatibility equations to determine the angle of the diagonal concrete struts. It should be noted that Mitchell and Collins (1974) developed a space truss model with concrete cover spalling to determine the shear flow zone thickness. Third, the softening phenomenon in the concrete struts, discovered by Robinson and Demorieux (1972), was quantified by Vecchio and Collins (1981) using a softened coefficient. Fourth, combining the equilibrium, compatibility, and softened stress-strain relationships, Hsu and Mo (1985a) developed a softened truss model (STM) theory to determine the shear and torsional behavior of reinforced concrete members throughout the post-crack loading history up to the peak strength. Using the STM theory, shear flow zone thickness t_d can be determined accurately to calculate the torsional strength of reinforced concrete members. The test data for solid and hollow beams suggests that, once cracking has occurred, concrete in the center member has little effect on torsional strength of the cross section and is ignored (Hsu 1968b; Lampert and Thürlimann 1968; Leonhardt and Schelling 1974). Beams are considered equivalent tubular members. This observation is the basis of the torsion design procedures introduced in ACI 318-95 (MacGregor and Ghoneim 1995).

5.2—Equilibrium conditions

5.2.1 *Shear elements in shear flow zone*—A prismatic reinforced concrete member subjected to an external torque T is shown in Fig. 5.2.1(a). This external torque is resisted by an internal torque formed by the circulatory shear flow q along the cross section periphery. This shear flow q occupies a zone, called the shear flow zone, with a thickness denoted by t_d. The thickness is a variable determined from equilibrium and compatibility conditions; it is different than the given wall thickness t of a hollow member.

An element A in the shear flow zone (Fig. 5.2.1(a)) is subjected to a shear stress $\tau_{\ell t} = q/t_d$, as shown in Fig. 5.2.1(b). The in-plane equilibrium of this element should satisfy Eq. (5.2.1a) through (5.2.1c) as originally derived by Nielsen (1967), Lampert and Thürlimann (1968, 1969), and Mitchell and Collins (1974), but given herein in the most general form (Hsu 1993)

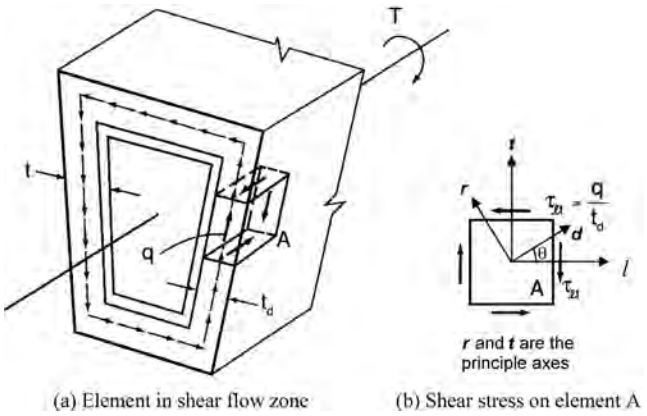


Fig. 5.2.1—Hollow box subjected to torsion (Hsu 1993).

$$\sigma_\ell = \sigma_d \cos^2\theta + \sigma_r \sin^2\theta + \rho_\ell f_\ell + \rho_{\ell p} f_{\ell p} \quad (5.2.1a)$$

$$\sigma_t = \sigma_d \sin^2\theta + \sigma_r \cos^2\theta + \rho_t f_t + \rho_{tp} f_{tp} \quad (5.2.1b)$$

$$\tau_{\ell t} = \left(-\sigma_d + \sigma_r\right)\sin\theta\cos\theta \quad (5.2.1c)$$

In Eq. (5.2.1a) through (5.2.1c) the reinforcement ratios ρ_ℓ, ρ_t, $\rho_{\ell p}$, and ρ_{tp}, should be taken with respect to the shear flow zone thickness t_d as described in 5.3. These three equations are expressed in the form of stress transformation to show that they satisfy Mohr's stress circle. Because Eq. (5.2.1a) and (5.2.1b) involve the reinforcement ratios ρ_ℓ, ρ_t, $\rho_{\ell p}$, and ρ_{tp}, they are coupled with the compatibility equations through the variable t_d. The thickness t_d is a geometric variable that is determined by equilibrium conditions as well as compatibility conditions. The determination of t_d is similar to that of the flexural neutral axis, which requires plane section compatibility conditions.

5.2.2 *Bredt's equilibrium equation*—Equations (5.2.1a) through (5.2.1c) were derived from the equilibrium of a member element in the shear flow zone. To maintain equilibrium of the whole cross section, a fourth equation derived by Bredt (1896) should be satisfied. For a shear flow zone thickness t_d, the shear stress $\tau_{\ell t}$ is

$$\tau_{\ell t} = \frac{T}{2A_o t_d} \quad (5.2.2)$$

This also introduces an additional variable, the torque T. The shear flow zone thickness t_d is incorporated in Eq. (5.2.2) explicitly, as well as implicitly through A_o, which is a function of t_d.

5.3—Compatibility conditions

5.3.1 *Shear elements*—As shown in Fig. 5.2.1(a), the element A in the shear flow zone is subjected to a shear

AVA Documents Document Sharing Hub
American Concrete Institute Copyrighted Material—www.concrete.org
Full document details: ACI 445.1R-12

stress. The in-plane deformation of this element should satisfy three compatibility equations (Eq. (5.3.1a) through (5.3.1c)) as originally derived by Baumann (1972) and Mitchell and Collins (1974). The equations are in the form of strain transformation to show they satisfy Mohr's strain circle (Hsu 1993)

$$\varepsilon_\ell = \varepsilon_d \cos^2\theta + \varepsilon_r \sin^2\theta \quad (5.3.1a)$$

$$\varepsilon_t = \varepsilon_d \sin^2\theta + \varepsilon_r \cos^2\theta \quad (5.3.1b)$$

$$\frac{\gamma_{\ell t}}{2} = \left(-\varepsilon_d + \varepsilon_r\right)\sin\theta\cos\theta \quad (5.3.1c)$$

Element A is subjected to in-plane shear as well as out-of-plane deformation as demonstrated (5.3.2).

5.3.2 *Shear strain due to twisting*—When a tube is subjected to torsion, the relationship between the shear strain $\gamma_{\ell t}$ in the tube wall and the member angle of twist, Φ, can be derived from the compatibility condition of warping deformation (Bredt 1896).

$$\Phi = \frac{p_o}{2A_o}\gamma_{\ell t} \quad (5.3.2)$$

It is clear from Eq. (5.3.2) that the angle of twist, Φ, will produce a shear strain $\gamma_{\ell t}$ in the shear flow zone elements. This shear strain $\gamma_{\ell t}$ will induce the reinforcement strains ε_ℓ and ε_t in the *d*-*r* direction. The relationships between the strains in the ℓ-*t* direction (ε_ℓ, ε_t, and $\gamma_{\ell t}$) and the strains in the *d*-*r* direction (ε_d and ε_r) are described by the three transformation equations, Eq. (5.3.1a) through (5.3.1c).

5.3.3 *Bending of diagonal concrete struts*—In a torsional member, the angle of twist, Φ, also produces warping in member walls that in turn causes bending in the concrete struts. The concrete struts are therefore subjected to compression due to circulatory shear and bending due to warping of walls. The relationship between the angle of twist, Φ, and the bending curvature of concrete struts, Ψ, is given in Eq. (5.3.3).

Figure 5.3.2(a) shows a box member with four walls of thickness *t* subjected to torsional moment *T*. Each wall contains a shear flow zone with a thickness of t_d. The perimeter of the centerline of shear flow *q* has a width of ℓ_q along the top wall. The length of the member in the longitudinal direction is taken to be $\ell_q\cos\theta$, so that the diagonal line in the center plane of the shear flow in the top wall OABC has an angle of inclination θ with respect to the longitudinal axis. When this member is subjected to an angle of twist, Φ, the center plane OABC becomes a hyperbolic paraboloid surface OADC, as shown in Fig. 5.3.2(b). The plane edge CB rotates to the position CD through an angle $\Phi\ell_q\cos\theta$.

The curve OD has a curvature of Ψ that is related to Φ and θ by

$$\Psi = \Phi\sin2\theta \quad (5.3.3)$$

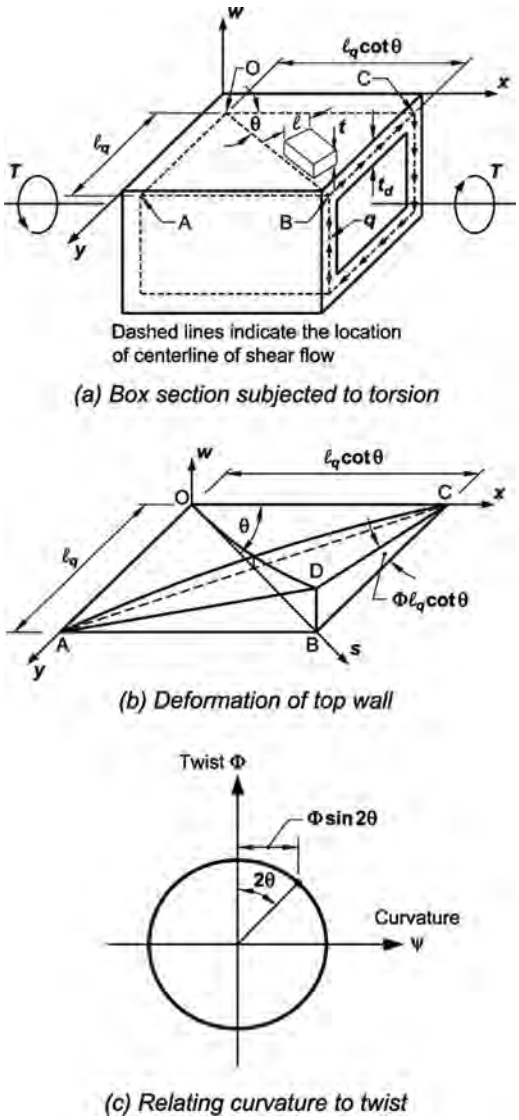


Fig. 5.3.2—Bending of a concrete strut in the wall of a box section subjected to torsion (Mitchell and Collins 1974; Hsu and Mo 1985a).

Equation (5.3.3) was originally derived by Mitchell and Collins (1974) using Mohr's circle, as shown in Fig. 5.3.2(c).

The illustration in Fig. 5.3.2 and the derivation of bending curvature are based on Hsu (1993). Although the imposed curvature is illustrated by a rectangular box section, this equation is applicable for any arbitrary, bulky section with multiple walls.

5.3.4 *Strain distribution in concrete struts*—The curvature Ψ derived in Eq. (5.3.3) produces a nonuniform strain distribution in the concrete struts. Figure 5.3.4(a) shows a concrete strut unit width in a hollow section with a wall thickness of *t*. The tension area in the cross section inner portion is disregarded. The area in the outer portion, which is in compression, is considered effective in resisting the shear flow. The compression zone depth from the neutral axis to the extreme compression fiber is defined as the shear flow zone thickness t_d. Within this thickness t_d, the strain distribution is assumed to be linear, as shown in Fig. 5.3.4(b), based on Bernoulli's

Documents Document Sharing Hub

American Concrete Institute Copyrighted Material—www.concrete.org

Full document details: ACI 445.1R-12

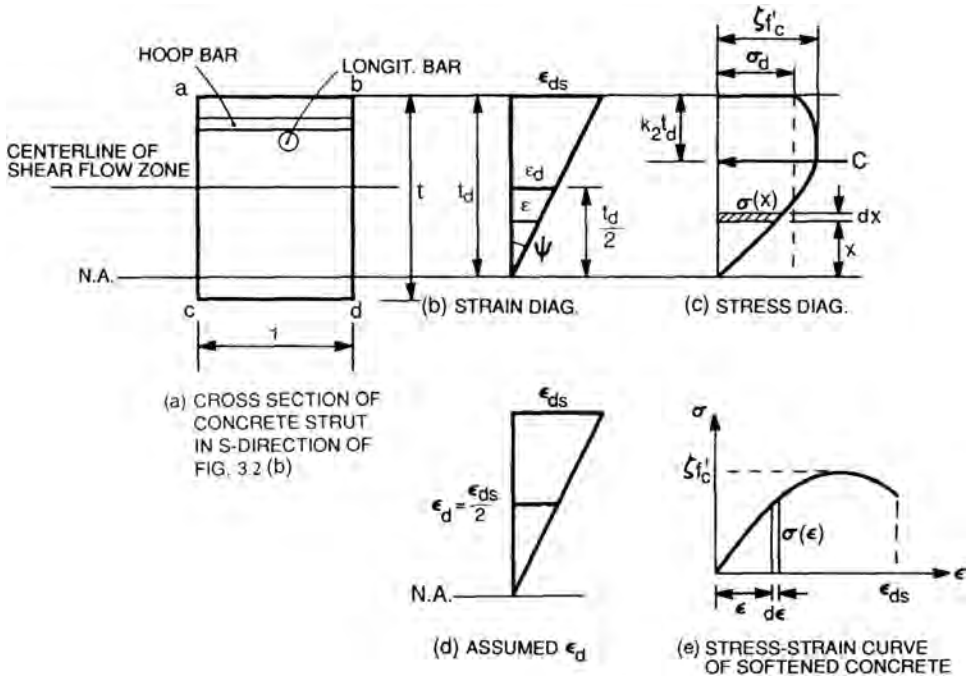


Fig. 5.3.4—Strains and stresses in concrete struts (Hsu and Mo 1985a).

plane section hypothesis used in bending theory (Mitchell and Collins 1974). The thickness t_d can therefore be related to the curvature Ψ and the maximum surface strain ε_{ds} by the simple relationship

$$t_d = \frac{\varepsilon_{ds}}{\Psi} \qquad (5.3.4a)$$

The average strain ε_d can be related to the maximum strain ε_{ds}, as shown in Fig. 5.3.4(d), by

$$\varepsilon_d = \frac{\varepsilon_{ds}}{2} \qquad (5.3.4b)$$

Equations (5.3.2), (5.3.3), (5.3.4a), and (5.3.4b) are the four additional compatibility equations for torsion. They introduce four additional variables, Φ, Ψ, t_d, and ε_{ds}.

5.4—Stress strain relationships

5.4.1 *Concrete struts*—The stress-strain relationship of concrete in compression, as shown in Fig. 5.3.4(e), can be expressed analytically by two branches of parabolic curves (Hsu and Mo 1985a)

Ascending branch:

$$\sigma_d = \zeta f_c' \left[2\left(\frac{\varepsilon_d}{\zeta\varepsilon_o}\right) - \left(\frac{\varepsilon_d}{\zeta\varepsilon_o}\right)^2 \right] \qquad \frac{\varepsilon_d}{\zeta\varepsilon_o} < 1 \qquad (5.4.1a(a))$$

Descending branch:

$$\sigma_d = \zeta f_c' \left[1 - \left(\frac{\varepsilon_d / \zeta\varepsilon_o - 1}{2/\zeta - 1} \right)^2 \right] \qquad \frac{\varepsilon_d}{\zeta\varepsilon_o} > 1 \qquad (5.4.1a(b))$$

where ζ is a softening coefficient. Section 5.6.1 discusses the softening coefficient as presented in Eq. (5.6.2d) with values ranging between 0.2 and 0.6.

The stress-strain relationship of concrete in tension is irrelevant, if the concrete tensile stress σ_r is assumed to be zero in the equilibrium Eq. (5.2.1a) through (5.2.1c).

5.4.2 *Mild reinforcement*—When the tensile strength of the concrete is neglected, the stress-strain relationship of mild reinforcement is taken as the elastic perfectly plastic relationship, expressed as

$$f_\ell = E_s\varepsilon_\ell \qquad \varepsilon_\ell < \varepsilon_{\ell y} \qquad (5.4.2a(a))$$

$$f_\ell = f_{\ell y} \qquad \varepsilon_\ell \geq \varepsilon_{\ell y} \qquad (5.4.2a(b))$$

$$f_t = E_s\varepsilon_t \qquad \varepsilon_t < \varepsilon_{ty} \qquad (5.4.2b(a))$$

$$f_t = f_{ty} \qquad \varepsilon_t \geq \varepsilon_{ty} \qquad (5.4.2b(b))$$

5.4.3 *Prestressing reinforcement*—In the case of prestressed concrete, the nonlinear stress-strain relationship of prestressed strands is given (Mattock 1979)

$$f_p = E_{ps}(\varepsilon_{dec} + \varepsilon_s) \qquad f_p \leq 0.7f_{pu} \qquad (5.4.3a(a))$$

Documents
Document Sharing Hub
American Concrete Institute Copyrighted Material—www.concrete.org
Full document details: ACI 445.1R-12

$$f_p = \frac{E'_{ps}(\varepsilon_{dec} + \varepsilon_s)}{\left[1 + \left\{\left(E'_{ps}(\varepsilon_{dec} + \varepsilon_s)\right) / f_{pu}\right\}^R\right]^{1/R}} \quad f_p > 0.7 f_{pu} \tag{5.4.3a(b)}$$

In structures where prestress is applied in both directions, such as nuclear containment vessels, Eq. (5.4.3a(a)) and (5.4.3a(b)) are applicable to prestressing reinforcement in both the longitudinal and transverse directions. When applied to longitudinal reinforcement, f_p is equal to f_{lp}, and ε_s is equal to ε_l. When applied to transverse reinforcement, f_p is equal to f_{tp}, and ε_s is equal to ε_t.

The equilibrium equations, compatibility conditions, and stress-strain relationships described are used by two main theories for torsional analysis, namely, the compression field theory (CFT) (Mitchell and Collins 1974) and the STM (Hsu and Mo 1985a). The primary difference between these two theories lies in the stress-strain relationship of concrete in compression. The STM uses a softened stress-strain curve as shown in Eq. (5.4.1a(a)) and (5.4.1a(b)), where ζ is a softening coefficient that varies from approximately 0.2 to 0.6. In CFT, the stress-strain curve is not softened, and the softening coefficients ζ in Eq. (5.4.1a(a)) and (5.4.1a(b)) are taken as unity. To compensate for the unconservative nature of this non-softening assumption, CFT also assumes spalling concrete cover before reaching the peak torque. As a result, CFT is also called the "spalling theory." The CFT and the STM are described in detail in 5.5 and 5.6, respectively, by combining the stress-strain relationships of concrete and reinforcement given in Eq. (5.4.1a(a)) and (5.4.1a(b)), and through (5.4.3a(b)) with the equilibrium Eq. (5.2.1a) through (5.2.1c) and (5.2.2) and compatibility Eq. (5.3.1a) through (5.3.4b). The solution algorithms of the two theories are also different.

5.5—Compression field theory

Collins and Mitchell (1980) and Mitchell and Collins (1974, 1978) proposed the CFT for structural concrete in torsion. This section provides a basic summary of the theory. Before the truss analogy equilibrium equations can be used to design a member for torsion, the diagonal struts' inclination should be determined from the compatibility equations. Wagner (1929) dealt with an analogous problem in studying the post-buckling shear resistance of thin-webbed metal girders. He assumed that after buckling, the thin webs would not resist compression and the shear would be carried by a field of diagonal tension. To determine the angle of inclination of the diagonal tension, Wagner considered the systems' deformations. He assumed that the angle of inclination of the diagonal tensile stress would coincide with the angle of inclination of the principal tensile strain. This approach became known as Tension Field Theory. Applying Wagner's approach to reinforced concrete, the concrete is assumed to be unable to carry tension, and the shear is assumed to be carried by a diagonal compression field. The inclination θ of the diagonal compression represents the principal strain

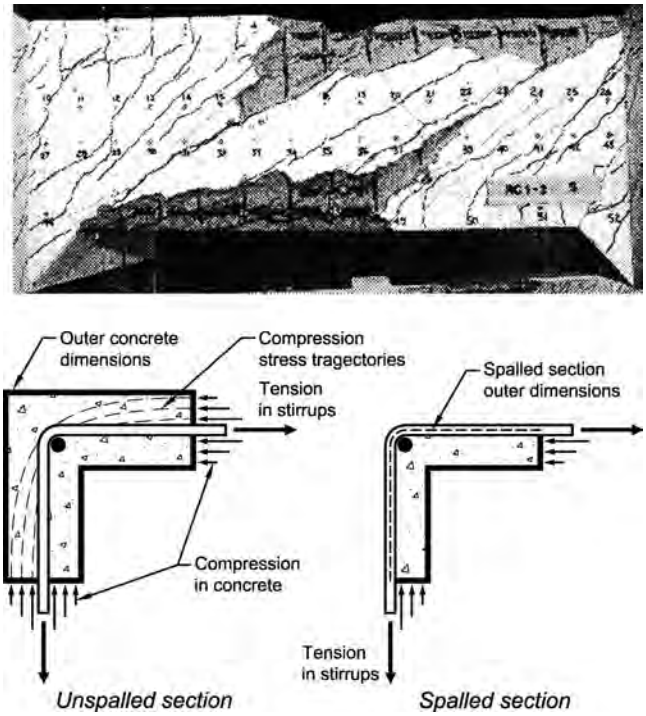


Fig. 5.5a—Spalling of the concrete cover due to torsion (Mitchell and Collins 1974).

direction; therefore, it can be derived from compatibility Eq. (5.3.1a) and (5.3.1b), by combining them to form

$$\tan^2\theta = \frac{\varepsilon_\ell + \varepsilon_d}{\varepsilon_t + \varepsilon_d} \tag{5.5a}$$

Equation (5.5a) shows the angle θ can be expressed as a function of the strain in the concrete diagonals (ε_d), the strain in the longitudinal reinforcement (ε_ℓ), and the strain in the transverse reinforcement (ε_t). The full behavioral response of reinforced concrete members subjected to torsion can be predicted by using compatibility (Eq. (5.5)), equilibrium (Eq. (5.2.1a) through (5.2.1c)), the stress-strain relationships of concrete [Eq. (5.4.1a(a)) and (5.4.1a(b))], and those for mild reinforcement [Eq. (5.4.2a(a)) through (5.4.2b(b))]. Besides these fundamental equations, additional torsional aspects were considered in the CFT. In resisting the torsion, not all of the concrete is effective in providing diagonal compressive stresses. Estimating the equilibrium of a corner element for a beam in torsion (Fig. 5.5a) reveals that the compression in the concrete tends to push off the corner whereas the tension in the hoops holds it in place. Because concrete is weak in tension, the concrete outside of the hoops spalls off at higher torsions. Because of concrete cover spalling, the effective outer surface of the concrete is assumed to coincide with the hoop centerline.

Examining the deformed shape of the twisted beam in Fig. 5.5b reveals that the diagonal concrete stresses vary in magnitude over the thickness of the effective concrete tube, from zero at the inside to a value f_{ds} corresponding to strain ε_{ds} at the effective outer surface. As in the case of

AVA Documents Document Sharing Hub

American Concrete Institute Copyrighted Material—www.concrete.org

Full document details: ACI 445.1R-12

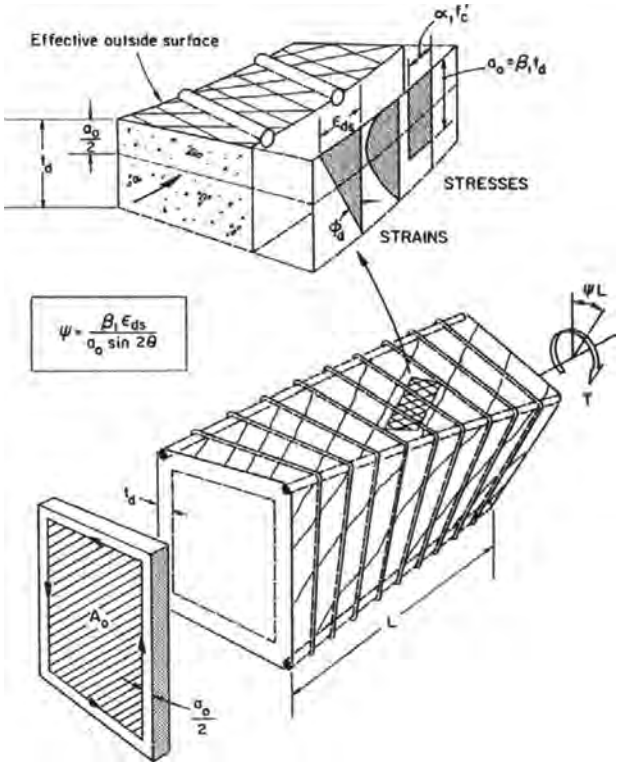


Fig. 5.5b—Effective wall thickness of a twisted beam (Collins and Mitchell 1980).

flexure, this actual stress distribution can be replaced by a uniform stress of $\alpha_1 f_c' = f_d$ acting over a depth of $\beta_1 t_d = a_o$, where the stress block factors α_1 and β_1 depend on the shape of the concrete stress-strain curve and the value of surface compression strain ε_{ds}. The centerline dimensions of the resulting tube of uniformly stressed concrete of thickness a_o are assumed to define the shear flow path q. This path lies $a_o/2$ inside the centerline of the hoop, as shown in Fig. 5.5b.

Given the shear flow path, the terms A_o (the area enclosed by the shear flow) and p_o (the perimeter of the shear flow path) can be determined using Eq. (5.5b) and (5.5c), which assume a thin tube

$$A_o = A_{oh} - \frac{a_o}{2} p_h \tag{5.5b}$$

$$p_o = p_h - 4a_o \tag{5.5c}$$

Based on the equilibrium of an element in the shear flow zone, shown in Fig. 5.2.1(b), the shear flow, q, in a box section can be expressed in terms of the longitudinal reinforcement force, ΔN, and the transverse reinforcement force, $A_t f_t$. The longitudinal reinforcement force ΔN is assumed to be distributed uniformly along the shear flow path p_o. Equilibrium Eq. (5.2.1a) through (5.2.1b) are simplified in three respects: 1) for pure torsion, $\sigma_\ell = \sigma_t = 0$; 2) concrete tensile stress is neglected, $\sigma_r = 0$; and 3) when no prestressing reinforcement is used, $\rho_{\ell p} = \rho_{tp} = 0$. In the CFT, several approximate algorithms have been developed to plot the torque-twist curve using the equilibrium and compatibility relationships given in 5.2 and 5.3. The following solution algorithm is the approach used by Rahal (2000a,b). From the equilibrium of an element in the shear flow zone, shown in Fig. 5.2.1(b), two equations can be derived

$$q = \sqrt{\frac{\Delta N}{p_o}\frac{A_t f_t}{s}} \tag{5.5d}$$

and

$$\tan\theta = \sqrt{\frac{A_t f_t}{s}\frac{p_o}{\Delta N}} \tag{5.5e}$$

Substituting Eq. (5.5d) into Bredt's Eq. (5.2.2), the torsional moment T can be related to the longitudinal and transverse reinforcement forces, ΔN and $A_t f_t$, as

$$T = 2A_o\sqrt{\frac{\Delta N}{p_o}\frac{A_t f_t}{s}} \tag{5.5f}$$

Like flexure, the compression zone depth is a function of reinforcement tensile forces, and is derived from equilibrium conditions. In a shear element, however, the reinforcement includes both longitudinal and transverse reinforcement forces, ΔN and $A_t f_t$. Eliminating θ from Eq. (5.2.1a) through (5.2.1c) results in

$$a_o = \frac{\Delta N}{\alpha_\ell f_c' p_o} + \frac{A_t f_t}{\alpha_1 f_c' s} \tag{5.5g}$$

Once the compression block depth a_o is known, the terms A_o and p_o in Eq. (5.5b) and (5.5c) can be calculated.

To determine the longitudinal and transverse beam strains, ε_l and ε_t, which correspond to the chosen value of ε_{ds}, the basic compatibility Eq. (5.3.1a) through (5.3.4a) were manipulated to develop two expressions

$$\varepsilon_t = \left[\frac{\alpha_1\beta_1 f_c' A_{oh} s}{2p_h A_t f_t} - 1\right]\varepsilon_{ds} \tag{5.5h}$$

$$\varepsilon_\ell = \left[\frac{\alpha_1\beta_1 f_c' A_{oh} p_o}{2p_h \Delta N} - 1\right]\varepsilon_{ds} \tag{5.5i}$$

A trial-and-error process can be used to solve the eight variables (θ, a_o, ε_t, ε_ℓ, A_o, p_o, ΔN, and $A_t f_t$) using Eq. (5.5a) through (5.5c), (5.5e), and (5.5h) through (5.5i). First, select a value of ε_{ds} and assume a pair of forces, $A_t f_t$ and ΔN, from which the four variables θ, a_o, ε_t, and ε_ℓ, can be calculated from Eq. (5.5e), (5.5g), (5.5h), and (5.5i), respectively. Given the value of a_o, the variables A_o and p_o can be calculated from Eq. (5.5b) and (5.5c). Based on the values of ε_t, ε_ℓ, and ε_d (related to ε_{ds} by geometry), another can be calculated from Eq. (5.5a). If the θ from Eq. (5.5a) is not equal

Documents Document Sharing Hub

American Concrete Institute Copyrighted Material—www.concrete.org

Full document details: ACI 445.1R-12

to the θ from Eq. (5.5e), assume another pair of $A_t f_t$ and ΔN, and repeat the cycle until Eq. (5.5a) and Eq. (5.5e) produce the same θ.

Once these eight variables are solved, the torque T can be calculated from Eq. (5.5f) and the angle of twist, Φ, from Eq. (5.3.3). In Eq. (5.3.3), the curvature of the concrete struts, Ψ, can be obtained from Eq. (5.3.4a), where the neutral axis depth t_d is equal to a_o/β_1, and ε_{ds} is the chosen value. The torque-twist response (T-versus-Φ curve) is then determined by repeating these calculations for a series of ε_{ds} values.

5.6—Softened truss model

5.6.1 *General*—The softened truss model is built on satisfying the equilibrium Eq. (5.2.1a) through (5.2.2), the compatibility Eq. (5.3.1a) through (5.3.4b), the stress-strain materials relationships in Eq. (5.4.1a(a)) and (5.4.1a(b)) for concrete, and Eq. (5.4.2a(a)) through (5.4.2b(b)) for reinforcement. The properties of concrete stress block and shear flow zone are derived from the softened stress-strain relationships of concrete.

5.6.2 *Concrete stress block*—As shown in Fig. 5.3.2, the diagonal concrete struts in the shear flow zone are subjected to axial stress and bending. The compressive strains in the concrete struts are assumed to vary linearly from ε_{ds} at the surface to zero at the neutral axis, as shown in Fig. 5.3.4(b). The compression zone depth t_d is defined as the shear flow zone. The distribution of compressive stresses within the thickness t_d is shown by the solid curve in Fig. 5.3.4(c), based on the softened stress-strain relationship shown in Fig. 5.3.4(e). The peak stress is $\zeta f_c'$ and the average compressive stress is σ_d. The average stress σ_d of the concrete stress block in Fig. 5.3.4(c) can be expressed as follows

$$\sigma_d = \zeta f_c' \tag{5.6.2a}$$

where the coefficient k_1 is the ratio of the average stress to the peak stress. By integrating the stress-strain curve in Eq. (5.4.1a(a)) and (5.4.1a(b)), the coefficient k_1 can be expressed

$$k_1 = \frac{\varepsilon_{ds}}{\zeta\varepsilon_o}\left(1-\frac{1}{3}\frac{\varepsilon_{ds}}{\zeta\varepsilon_o}\right) \qquad \frac{\varepsilon_{ds}}{\varepsilon_p} \le 1 \tag{5.6.2b(a)}$$

$$k_1 = \left[1-\frac{\zeta^2}{(2-\zeta)^2}\right]\left(1-\frac{1}{3}\frac{\varepsilon_{ds}}{\zeta\varepsilon_o}\right)+\frac{\zeta^2}{(2-\zeta)^2}\frac{\varepsilon_{ds}}{\zeta\varepsilon_o}\left(1-\frac{1}{3}\frac{\varepsilon_{ds}}{\zeta\varepsilon_o}\right) \qquad \frac{\varepsilon_{ds}}{\varepsilon_p} > 1 \tag{5.6.2b(b)}$$

The coefficient k_1 is tabulated as a function of ε_{ds} and ζ in the work by Hsu (1993), and equals approximately 0.8. The softening coefficient was first proposed by Zhang and Hsu (1998) as a function of tensile strain ε_r and concrete strength f_c'

$$\zeta = \frac{5.8}{\sqrt{f_c'(\text{MPa})}}\frac{1}{\sqrt{1+400\varepsilon_r}} \quad \text{and} \quad \frac{5.8}{\sqrt{f_c'(\text{MPa})}} \le 0.9 \tag{5.6.2c}$$

This equation is valid for HSC up to 100 MPa (14.5 ksi). As proposed by Belarbi and Hsu (1995), for NSC up to 42 MPa (6.0 ksi), ζ becomes

$$\zeta = \frac{0.9}{\sqrt{1+400\varepsilon_r}} \tag{5.6.2d}$$

The softening coefficient ζ usually varies in the range of 0.2 (0.045) to 0.6 (0.003).

5.6.3 *Centerline of shear flow zone and formulas for* A_o and p_o—As shown in Fig. 5.3.4(c), the resultant force of the compression stress block C is located at a distance $k_2 t_d$ from the surface, where the coefficient k_2 defines the location of the resultant force C. By integrating the concrete stress-strain curve given in Eq. (5.4.1a(a)) and (5.4.1a(b)), the coefficient k_2 is found to vary in the range of 0.40 to 0.45, depending on concrete strength. To simplify, the centerline of the shear flow is assumed to coincide with the centerline of the shear flow zone, located at a distance $0.5t_d$ from the extreme compression fiber. This assumption also results in a compatible agreement between theory and tests.

Based on this simple centerline assumption of the shear flow, formulas for calculating the lever arm area A_o and the perimeter p_o for a thick tube, whose thickness is usually quite large with respect to the overall dimension of the cross section and different from the thin tube assumption in CFT when the softening of concrete is considered, are

$$A_o = A_c - \frac{1}{2}p_c t_d + t_d^2 \tag{5.6.3a}$$

$$p_o = p_c - 4t_d \tag{5.6.3b}$$

When the softening coefficient ζ of concrete is considered, the shear flow zone thickness t_d is usually large with respect to the overall cross section dimensions. The formula for calculating A_o, therefore, is expressed in Eq. (5.6.3a) and should include the third term t_d^2. The thin tube formula used in the CFT (Eq. (5.5b)) is not used because it neglects the a_o^2 term.

5.6.4 *Solution algorithm*—The 18 governing equations for a torsional member are: four equilibrium, (Eq. (5.2.1a) through (5.2.2); seven compatibility, (Eq. (5.3.1a) through (5.3.4b)); seven constitutive (Eq. (5.4.2a(a)) through (5.4.3a(b)) and (5.6.2a) through (5.6.2d)).

For a member subjected to pure torsion, the normal stresses σ_ℓ and σ_t acting on an element in the shear flow zone are equal to zero ($\sigma_\ell = \sigma_t = 0$). When the concrete tensile strength is neglected, $\sigma_r = 0$. Disregarding these three variables (σ_ℓ, σ_t, and σ_r) in the analysis, the 18 equations contain 19 unknown variables as follows: seven stress or force variables, including $\tau_{\ell t}$, σ_d, f_ℓ, f_t, $f_{\ell p}$, f_{tp}, and T; 10 strain or geometry variables, including ε_ℓ, ε_t, $\gamma_{\ell t}$, ε_d, ε_r, θ, Φ, Ψ, t_d, and ε_{ds}; and two material coefficients, including ζ and k_1. If one of the unknown variables is selected—for example, ε_d—then the remaining 18 unknown variables can be solved using the 18 equations.

Document Sharing Hub

American Concrete Institute Copyrighted Material—www.concrete.org

Full document details: ACI 445.1R-12

Next, select the concrete strain ε_d as the independent variable because it varies monotonically from zero to maximum. The solutions for a series of ε_d values make it possible to trace the loading history. A solution algorithm is given by Hsu (1993) and is briefly described. This method requires the derivations of Eq. (5.6.5) through (5.6.8b).

5.6.5 *Thickness* t_d *as a function of strain*—The thickness of the shear flow zone t_d can be expressed in terms of strain using the seven compatibility equations: Eq. (5.3.1a) through (5.3.4b). The substitutions and manipulations result in

$$t_d = \frac{A_o}{p_o}\left[\frac{(-\varepsilon_d)(\varepsilon_r - \varepsilon_d)}{(\varepsilon_\ell - \varepsilon_d)(\varepsilon_t - \varepsilon_d)}\right] \tag{5.6.5}$$

The variable t_d is expressed in terms of strains in all d, r, ℓ, and t directions (ε_d, ε_r, ε_ℓ, ε_t). The compressive strain is defined as negative and tensile as positive. The variable t_d is also involved in equilibrium equations through the terms A_o, p_o, ρ_ℓ, and ρ_t. Therefore, the variable t_d should first be assumed and then checked by Eq. (5.6.5).

5.6.6 *Longitudinal strain* ε_l *as a function of longitudinal stresses* f_ℓ, $f_{\ell p}$—The strain ε_ℓ can be related to the reinforcement stresses f_ℓ and $f_{\ell p}$ by eliminating the angle α from the equilibrium Eq. (5.2.1a) using compatibility equations (Eq. (5.3.1c) to (5.3.4b)). These manipulations result in

$$\varepsilon_\ell = \varepsilon_d + \frac{A_o(-\varepsilon_d)(-\sigma_d)}{(A_\ell f_\ell + A_{\ell p} f_{\ell p})} \tag{5.6.6}$$

The three unknown variables ε_ℓ, f_ℓ, and $f_{\ell p}$ can be solved using Eq. (5.6.6) and the stress-strain relationships, Eq. (5.4.2a), (5.4.2b), (5.4.3a), and (5.4.3b), for longitudinal reinforcement.

5.6.7 *Transverse strain* ε_t *as a function of transverse stresses* f_t, f_{tp}—Similarly, the strain ε_t can be related to the reinforcement stresses f_t and f_{tp} by eliminating the angle θ from equilibrium Eq. (5.2.1b) using the compatibility equations (Eq. (5.3.1b) through (5.3.4b)).

$$\varepsilon_t = \varepsilon_d + \frac{A_o s(-\varepsilon_d)(-\sigma_d)}{p_o(A_t f_t + A_{tp} f_{tp})} \tag{5.6.7}$$

The three unknown variables ε_t, f_t, and f_{tp} can be solved using Eq. (5.6.7) and the two stress-strain relationships, Eq. (5.4.2c) and (5.4.2d) and (5.4.3a) and (5.4.3b), for transverse reinforcement.

5.6.8 *Useful compatibility equations*—By combining compatibility Eq. (5.3.1a) and (5.3.1b), the two variables ε_r and θ can be expressed directly in terms of strains ε_ℓ, ε_t, and ε_d as

$$\varepsilon_r = \varepsilon_\ell + \varepsilon_t - \varepsilon_d \tag{5.6.8a}$$

$$\tan^2\theta = \frac{\varepsilon_\ell + \varepsilon_d}{\varepsilon_t + \varepsilon_d} \tag{5.6.8b}$$

Equations (5.6.8a) and (5.6.8b) will facilitate solution procedures (5.6.9).

5.6.9 *Solution procedure and flow chart*—The solution procedure is illustrated by a flow chart shown in Fig. 5.6.9. This solution procedure uses 12 equations, Eq. (5.4.2a) through (5.4.3b) and (5.6.2a) through (5.6.8b), to solve 12 unknown variables (ζ, k_1, σ_d, f_ℓ, f_t, $f_{\ell p}$, f_{tp}, ε_ℓ, ε_t, ε_r, ε_{ds}, and t_d) for each selected value of ε_d. From these stresses and strains, the remaining six variables (θ, $\tau_{\ell t}$, T, $\gamma_{\ell t}$, Φ, Ψ) can be calculated using the appropriate equilibrium or compatibility equations. Selecting a series of ε_d values produces the entire loading history of the 18 variables. The efficiency of this solution procedure arises from the fact that the angle θ is eliminated in the expressions of Eq. (5.6.5) through (5.6.7) and is, therefore, not involved in the iteration process of t_d. In addition, the derivation of Eq. (5.6.6) and (5.6.7) allows the iteration to include nonlinear stress-strain relationships (Eq. (5.4.3a) and (5.4.3b)) of prestressing strands, therefore making this solution algorithm applicable to prestressed concrete beams. A hand-calculation example illustrating this solution procedure is given by Hsu (1993). The STM theory was used by Hsu and Mo (1983, 1985a) to calculate the strength and behavior of 108 torsional beams. For the 61 under-reinforced beams with stirrup spacings within ACI code limits, the experiment-to-calculated torsional strengths had a mean value of 1.014 and a standard deviation of 0.051. The post-cracking deformations (angle of twist and strains in reinforcement and concrete) were also correctly evaluated. McMullen and El-Degwy (1985) compared the STM (softened theory) and the CFT (spalling theory) using their extensive torsion tests. They concluded that "the space truss model with softening of concrete gives a better prediction of maximum torque for the beams tested in this investigation (average $T_{u,exp}/T_{u,th}$ = 1.03 and standard deviation = 0.091)." The space truss theory with spalling of concrete cover gave an average $T_{u,exp}/T_{u,th}$ of 1.10 and a standard deviation of 0.129. McMullen and El-Degwy also observed that concrete cover spalled only after maximum torque was reached.

5.7—Graphical methods

5.7.1 *Rahal's method*—Rahal developed a simplified method for design and analysis of reinforced concrete panels subjected to pure shear (Rahal 2000a) and extended the method to reinforced concrete beams subjected to torsional moments (Rahal 2000b). The original method for calculating shear relates the normalized ultimate shear strength v_u/f_c' of reinforced concrete panels to the reinforcement indexes ω_t and ω_L in the transverse and longitudinal directions, respectively. The reinforcement indexes are given by

$$\omega_t = \frac{\rho_t f_{ty}}{f_c'}; \quad \omega_L = \frac{\rho_\ell f_{\ell y}}{f_c'} \tag{5.7.1a}$$

Figure 5.7.1 gives the relationship between the indices and the normalized shear strength obtained using the results of the modified CFT (Collins and Mitchell 1991). Each curve

Document Sharing Hub
American Concrete Institute Copyrighted Material—www.concrete.org
Full document details: ACI 445.1R-12

in the figure represents the relationship between v_u/f_c' and ω_L at a given ω_t.

At relatively low ω_t values, the strains in the transverse reinforcement exceed the yield strains before the ultimate strength is reached. Beyond a specific level of reinforcement, the concrete is crushed before the reinforcement yields. Figure 5.7.1 shows a curve passing through those points beyond which concrete is crushed before the transverse reinforcement yields (over-reinforced case). The figure also shows a similar curve for the over-reinforced case in the longitudinal direction. The two "yield" curves divide Fig. 5.7.1 into four regions. The relative position of a point of coordinates (ω_t; ω_L), with respect to these curves or regions, indicates the expected failure mode of an element with these reinforcement ratios. Four failure modes are possible:

1) Partially over-reinforced; only longitudinal reinforcement yields (Zone III)

2) Only transverse reinforcement yields (Zone II)

3) Completely over-reinforced; concrete crushing before reinforcement yielding (Zone IV) or

4) Completely under-reinforced; longitudinal and transverse reinforcement yield (Zone I).

- Because v_u/f_c', ω_t, and ω_L are dimensionless, they provide values that can be applied to any system of units. The results of this method have been compared with experimental results from 46 reinforced concrete panels and were found to give accurate calculations of the ultimate shear strength and failure mode. The average ratio of experimental shear strength to predicted strength was 1.01 with a coefficienct of variation (COV) of 0.125 (Rahal 2000a). This method is applied to beams subjected to torsion by idealizing the section as a hollow tube and adopting simplified assumptions regarding the hollow tube thickness and shear flow zone size. Tube walls are treated as the shear panels to which Fig. 5.7.1 applies. Based on assumptions of the method, the reinforcing indexes are given by

$$\omega_t = \frac{A_t f_{ty} p_o}{0.42 s A_{cp} f_c'} \qquad (5.7.1b)$$

$$\omega_L = \frac{A_\ell f_{\ell y} + A_{ps} f_{py}}{0.375 s A_{cp} f_c'} \qquad (5.7.1c)$$

The ultimate torsional moment is also related to ultimate shear strength in walls

$$T_u = 0.67 \frac{A_{cp}^2}{p_{cp}} v_u \qquad (5.7.1d)$$

In contrast to the STM and CFT, Rahal's method is used to calculate approximate strength only and not the entire torque-twist relationship. Equations (5.7.1b), (5.7.1c), and (5.7.1d) depend on the gross area and outer cross section perimeter, and therefore can be applied to closed sections of various shapes.

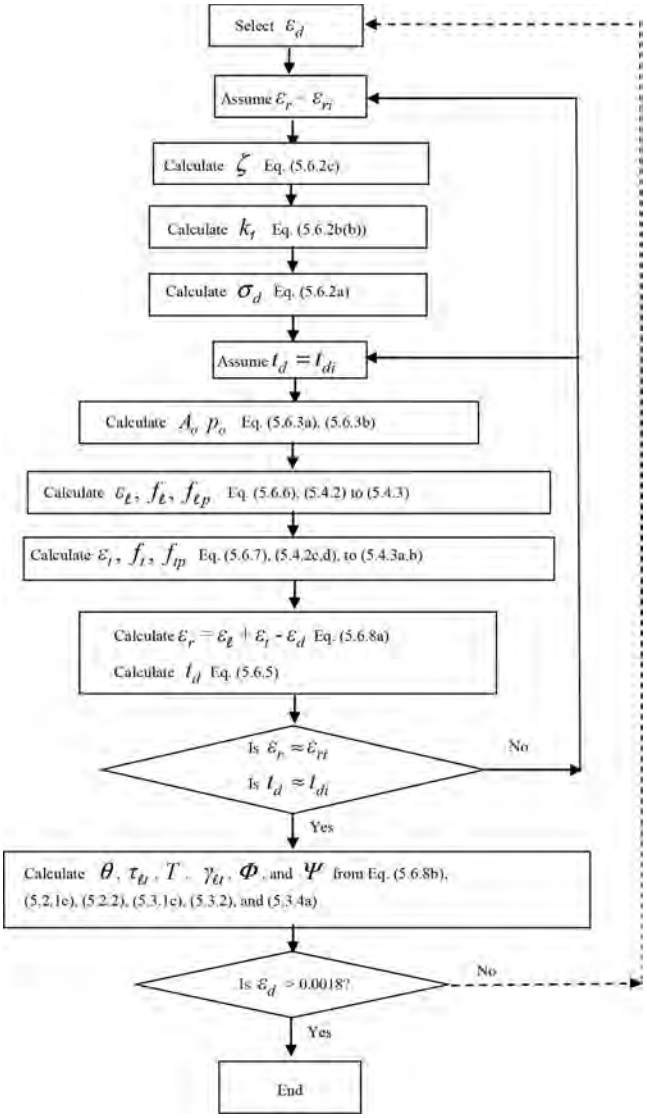


Fig. 5.6.9—Flow chart for torsion analysis using STM.

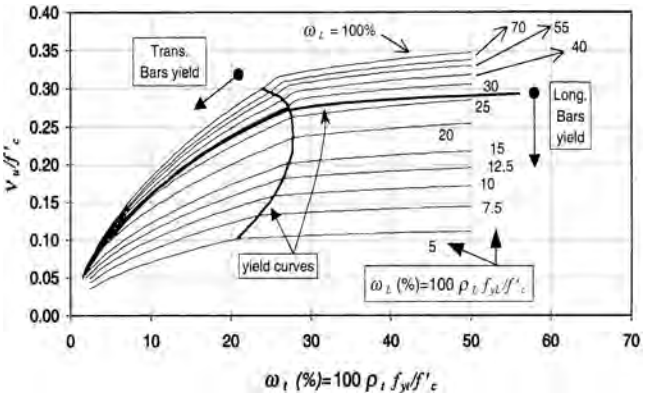


Fig. 5.7.1—Normalized shear strength curve for reinforced concrete members (Rahal 2000a).

5.7.2 *Leu and Lee's Method*—Leu and Lee (2000) proposed a graphical solution to the STM. Their strength

American Concrete Institute Copyrighted Material—www.concrete.org

Full document details: ACI 445.1R-12